Pergamon

J. Mech. Phys. Solids, Vol. 45, No. 6, pp. 1037–1067, 1997

0022–5096/97 $17.00+0.00

PII: S0022–5096(96)00114–7

DESIGN OF MATERIALS WITH EXTREME THERMAL EXPANSION USING A THREE-PHASE TOPOLOGY OPTIMIZATION METHOD

O. SIGMUND* and S. TORQUATO

Department of Civil Engineering and Operations Research and Princeton Materials Institute, Princeton University, Princeton, NJ 08544, U.S.A.

(*Received* 27 *May* 1996)

ABSTRACT

Composites with extremal or unusual thermal expansion coefficients are designed using a three-phase topology optimization method. The composites are made of two different material phases and a void phase. The topology optimization method consists in finding the distribution of material phases that optimizes an objective function (e.g. thermoelastic properties) subject to certain constraints, such as elastic symmetry or volume fractions of the constituent phases, within a periodic base cell. The effective properties of the material structures are found using the numerical homogenization method based on a finite-element discretization of the base cell. The optimization problem is solved using sequential linear programming.

To benchmark the design method we first consider two-phase designs. Our optimal two-phase microstructures are in fine agreement with rigorous bounds and the so-called Vigdergauz microstructures that realize the bounds. For three phases, the optimal microstructures are also compared with new rigorous bounds and again it is shown that the method yields designed materials with thermoelastic properties that are close to the bounds.

The three-phase design method is illustrated by designing materials having maximum directional thermal expansion (thermal actuators), zero isotropic thermal expansion, and negative isotropic thermal expansion. It is shown that materials with effective negative thermal expansion coefficients can be obtained by mixing two phases with positive thermal expansion coefficients and void. © 1997 Elsevier Science Ltd

Keywords: A. microstructures, A. thermomechanical processes, B. constitutive behavior, C. numerical algorithms, C. optimization.

1. INTRODUCTION

In this paper, we use a topology optimization procedure to determine the distribution of three phases (two different bulk material phases and a void phase) in order to design composites with extremal or unusual thermal expansion behavior. Three phases are used (as opposed to two phases) since one can achieve effective properties of the composite beyond those of the individual components (Lakes, 1993). Microstructural variation is limited to one length scale in a unit cell as this is most easily manufacturable.

* Partly on leave from Department of Solid Mechanics, Technical University of Denmark, DK-2800 Lyngby, Denmark (current and permanent address).

Materials with extreme or unusual thermal expansion behavior are of interest from both a technological and fundamental standpoint. Of particular practical interest are materials with zero thermal expansion, maximum thermal expansion or force, and negative (i.e. minimum) thermal expansion. Heretofore, however, a systematic procedure to design materials with exotic thermal-expansion behavior has been lacking.

Materials with *zero thermal expansion coefficients* are needed for use in structures subject to temperature changes such as civil engineering and space structures as well as piping systems. Examples are bridges, where temperature changes between day and night, and summer and winter, cause big structural changes, and space applications, where temperature differences between sunny and shady sides of a structure are extreme. Such temperature differences can cause distortion of space antennas and "rapid" temperature changes due to orbit of the Hubble space telescope are known to cause thermal distortions of its solar arrays in turn causing the arrays and thereby the telescope to vibrate (Collins and Richter, 1995). Materials with *maximum unidirectional thermal displacement or force* can be employed as "thermal" actuators. Materials with negative thermal expansion coefficients can be used to overcome positive thermal expansion of other materials or, among other applications, be used for thermally operated fasteners. A fastener made of a negative thermal expansion coefficient material, upon heating, can be inserted easily into a hole because of the volume contraction. When cooled down, it will expand, fitting tightly into the hole and upon heating can be easily removed. Finally, the design of material with specific thermal expansion coefficients is important, to be able to eliminate thermal mismatch between parts in structures subject to heat changes.

A negative thermal expansion material has the counterintuitive property of contracting upon heating. There are a number of existing materials with negative thermal expansion coefficients. Glasses in the titania–silica family have isotropic negative expansion coefficients at *room temperature* (Schultz and Smyth, 1970). Examples of materials that have negative thermal expansion at very low temperatures (< 100 K) are silicon and germanium (Kagaya and Soma, 1993) as well as $Bi_{2.2}Sr_{1.8}CaCu_2O_x$ superconductor single crystals (Yang *et al.*, 1995). Examples of materials with *directional* negative thermal expansion coefficients at room temperature are Kevlar, carbon fibers, plastically deformed (anisotropic) Invar (Fe–Ni alloys) (Hausch *et al.*, 1989) and certain molecular crystalline networks (Baughman and Galvão, 1993). The negative expansion mechanism of these molecular-level networks is based on untwisting of helical chains. Currently there is no way to manufacture these materials in extended form, but this is an active area of research.

An interesting question (Baughman and Galvão, 1993) is whether there is a mechanistic relationship between negative thermal expansion and negative Poisson's ratio? A material with negative Poisson's ratio expands laterally when pulled axially and can be manufactured by processing of open-walled foam structures described by Lakes (1987). We will show that isotropic materials with effective negative thermal expansion coefficients exist with positive values of the Poisson's ratio and that they can be obtained by mixing two phases with positive thermal expansion coefficients and void.

Several researchers have addressed the problem of designing materials composites

with specific *directional* thermal expansion properties. Autio *et al.* (1993) designed laminates with specific elastic and thermal expansion coefficients by varying layering thicknesses and directions. Wetherhold and Wang (1995) tailored the thermal deformation of beams, and Parton and Kudryavtsev (1993) discussed the design of one dimensional beams with negative thermal expansion. Rodriques and Fernandes (1995) designed thermally loaded structures with optimal stiffness.

It was shown by Levin (1967) and later by Rosen and Hashin (1970), that there is a simple relationship between the effective thermal expansion coefficients and the effective elastic moduli of *two-phase* materials. In other words, designing two-phase composites with extreme thermal expansion coefficients corresponds to designing two-phase composites with extreme bulk moduli. The problem of finding the structures that extremize the effective elastic properties of two-phase media has a long history beginning with the composite-sphere assemblages of Hashin and Shtrikman (1963) for the bulk modulus problem. Certain hierarchical laminates were shown to realize the Hashin–Shtrikman bounds on both the bulk and shear moduli of isotropic two-phase composites (Franckfort and Murat, 1986). More recently, Milton and Cherkaev (1995) have found multi-length scale materials possessing elastic properties ranging over the entire range compatible with thermodynamics. Vigdergauz (1989, 1994) and Grabovsky and Kohn (1995a, b) have studied single-inclusion microstructures of extreme rigidity. Sigmund (1994a, b, 1995) has designed material structures with specific elastic properties (including isotropic negative Poisson's ratio material), where the microstructure is restricted to one length scale.

For three-phase materials, one-to-one relationships between the thermal expansion coefficients and elastic properties do not exist. Indeed, for multiphase composites, Schapery (1968) and Rosen and Hashin (1970) found bounds on the thermal expansion coefficients in terms of the stiffness tensor. Recently, Gibiansky and Torquato (1997) have improved upon the Rosen–Hashin bounds using the so-called translation method. This improvement was actually motivated by the topology optimization results of the present study. To our knowledge, no one to date has addressed the problem of systematically designing three-phase materials with extreme *isotropic* thermal expansion coefficients.

In this paper, we show how composites with extremal or unusual thermal expansion coefficients can be designed using a three-phase topology optimization method based on the aforementioned works of Sigmund. The three phases consist of two different material phases and void. The two material phases can have different elastic and thermal expansion coefficients, described by their elastic tensors $C^{(1)}_{ijkl}$ and $C^{(2)}_{ijkl}$ and their thermal strain coefficient tensors $\alpha^{(1)}_{ij}$ and $\alpha^{(2)}_{ij}$, respectively. The basic goal is to maximize or minimize components, or combination of components, of the effective thermal strain tensor $\alpha^{(*)}_{ij}$ or effective stress tensor $\beta^{(*)}_{ij} = C^{(*)}_{ijkl}\alpha^{(*)}_{kl}$, subject to constraints on phase volume fractions, effective stiffness and elastic symmetry. To check the validity of the optimization procedure, our results will be compared with the available bounds on thermoelastic properties for three-phase materials (Schapery, 1968; Rosen and Hashin, 1970; Gibiansky and Torquato, 1997).

The topology optimization procedure proposed here, essentially follows the steps of conventional topology optimization procedures. The design problem is initialized by defining a design domain discretized by a number of finite elements. The opti-

mization procedure then consists of solving a sequence of finite-element problems followed by changes in density and material type of each of the finite elements, dependent on the local strain energies. For simple compliance optimization, this corresponds to adding material where the strain energy density is high and removing material where the strain energy density is low.

The proposed procedure differs from the conventional approach in an important aspect. In the original works on topology optimization [e.g. Kohn and Strang (1986), Bendsøe and Kikuchi (1988) and Bendsøe (1995) for an overview of methods], elimination of ill-conditioning and the existence of materials in elements of intermediate densities was ensured by using so-called ranked materials made of microscopically oscillating material on differing length scales or by using microstructures with rectangular holes. Using homogenization methods to determine the effective properties of ranked (or microstructured) materials and substituting the homogenized parameters into the "macroscopic" topology optimization problem, lead to the "homogenization approach to topology optimization". In this paper, however, we will use an "artificial" material model for intermediate densities which means that the material properties in a given element are simply some fraction times the material properties of solid material. As long as we end up having entirely solid material or void in each element, this is a perfectly valid approach. By using the "artificial-material" model, we simplify the whole design procedure significantly because the local problems of determining lamination parameters and orientations at different length scales of the ranked materials are eliminated. The "artificial-material" model has been used by several authors (e.g. Rozvany *et al.*, 1992; Mlejnek and Schirrmacher, 1993; Sigmund, 1994a).

At each step of the topology optimization procedure, we have to determine the effective thermoelastic properties of the microstructure. There exist several methods to determine these properties. However because the topology optimization method is based on finite-element discretizations, and because the finite-element method allows easy derivation and evaluation of the sensitivities of the effective properties with respect to design changes, we have chosen to use a finite element based numerical homogenization procedure as developed in Bourgat (1977) and Guedes and Kikuchi (1991).

The paper is organized the following way. In Section 2 we describe the three-phase topology optimization procedure and its application to design of material structures with extreme thermal expansion. The sequential linear programming method used to solve the topology optimization problem is described in Section 2.2 and numerical implementation issues are discussed in Section 2.3. Solving the topology optimization procedure as proposed, results in solutions with finite-element related problems such as checkerboards, mesh-dependency and local optima. These problems and procedures to avoid them are discussed in Section 2.4. To benchmark the optimization procedure, results obtained are compared to bounds for two- and three-phase materials; the available bounds are listed in Section 3. The performance of the design procedure is demonstrated by several examples in Section 4. The calculation of the effective thermoelastic properties using a numerical homogenization procedure based on the finite-element method is briefly described in Appendix A and the sensitivity analysis necessary to solve the design problem is listed in Appendix B.

2. PROCEDURES FOR THREE-PHASE TOPOLOGY OPTIMIZATION

This section describes a numerical procedure for topology optimization of three-phase material structures in two dimensions. A sequential linear programming problem is formulated to solve the optimization problem. The procedure is applied to the design of material structures with extreme thermal expansion properties. For the derivations, we will assume that we can find the effective stiffness and thermal expansion tensors $C^{(*)}_{ijkl}$, $\alpha^{(*)}_{ij}$ and $\beta^{(*)}_{ij}$ using the numerical homogenization method described in Appendix A. The sensitivity analysis necessary for solving the problem is derived in Appendix B. At the end of the section, we discuss implementation issues as well as some numerical difficulties and how to avoid them.

Assuming two-dimensional linear elasticity (i.e. small strains), perfect bonding between the material phases, uniform temperature distribution and constant material properties, the thermoelastic behavior of materials can be described by the constitutive relations given as

$$\sigma_{ij} = C_{ijkl}\varepsilon_{kl} - C_{ijkl}\alpha_{kl}\Delta T = C_{ijkl}\varepsilon_{kl} - \beta_{ij}\Delta T, \tag{1}$$

where C_{ijkl}, σ_{ij}, ε_{kl}, α_{kl}, β_{ij} are the elasticity, stress, strain, thermal strain and thermal stress tensors, respectively, and ΔT is the temperature change. We refer to α_{kl} as the "thermal strain tensor" (the resulting strain of a material which is allowed to expand freely and which is subjected to increase in temperature of one unit) and to β_{ij} as the "thermal stress tensor" (the stress in a material which is not allowed to expand and which is subjected to increase in temperature of one unit). For the three-phase composite of interest, the constitutive equation (1) is valid on a local scale [with superscripts (0), (1), and (2) appended to the thermoelastic properties, i.e. $C^{(m)}_{ijkl}$, $\alpha^{(m)}_{ij}$ and $\beta^{(m)}_{ij}$) and the macroscopic scale (with superscript (*) appended to the properties). In the latter case, the stresses and strains are averages over local stresses and strains, respectively, i.e.

$$\bar{\sigma}_{ij} = C^{(*)}_{ijkl}\bar{\varepsilon}_{kl} - C^{(*)}_{ijkl}\alpha^{(*)}_{kl}\Delta T = C^{(*)}_{ijkl}\bar{\varepsilon}_{kl} - \beta^{(*)}_{ij}\Delta T, \tag{2}$$

where overbar denotes the volume average. The effective thermoelastic properties, $C^{(*)}_{ijkl}$, $\alpha^{(*)}_{kl}$ and $\beta^{(*)}_{ij}$ of the three-phase composite are computed using a numerical homogenization method as described in Appendix A.

The goal of this work is to optimize components or combinations of components of the effective thermal tensors $\alpha^{(*)}_{ij}$ or $\beta^{(*)}_{ij}$ by distributing, in a clever way, given amounts of two material phases and void within the design domain representing a base cell of a periodic material. In other words, we want to design microstructural topologies that give us some desirable overall thermoelastic properties. As will be seen later, materials with extreme thermal expansion tend to have low overall stiffness. Thus, for practical applications, one must bound the effective stiffness or bulk moduli from below. It should also be possible to specify elastic symmetries such as orthotropy, square symmetry or isotropy of the resulting materials.

An optimization problem including these features can be written as:

Minimize: some function of $\alpha_{ij}^{(*)}$ or $\beta_{ij}^{(*)}$;

Variables: distribution of two material phases and void in the base cell;

Subject to: constraints on volume fractions;

orthotropy, square symmetry or isotropy constraints;

lower bound constraints on stiffness;

bounds on design variables. (3)

2.1. *Formulation of the optimization problem*

This subsection discusses the individual parts of the optimization problem defined in (3).

Objective function. The objective function $f(\alpha_{ij}^{(*)}, \beta_{ij}^{(*)})$ can be any combination of the thermal coefficients $\alpha_{ij}^{(*)}$ or $\beta_{ij}^{(*)}$. An example will be the case where we want to minimize the isotropic thermal expansion, i.e. the sum of the thermal strain coefficients in the horizontal and the vertical directions. In that case, the objective function will be $f(\alpha_{ij}^{(*)}) = \alpha_{11}^{(*)} + \alpha_{22}^{(*)}$, where subscripts 11 and 22 define horizontal and vertical directions, respectively. As another example we might consider the maximization of the thermal stress coefficient in the vertical direction. In this case, the objective function will be $f(\beta_{ij}^{(*)}) = -\beta_{22}^{(*)}$ where the minus sign is used to convert the maximization problem into a minimization problem.

Design variables and mixture assumption. Phase 1 material has the stiffness tensor $C_{ijkl}^{(1)}$ and the thermal strain coefficient tensor $\alpha_{ij}^{(1)}$ and similarly phase 2 material has the material tensors $C_{ijkl}^{(2)}$ and $\alpha_{ij}^{(2)}$. The stiffness tensor of the "void" phase is taken as a small number $x_{\min}$ times $C_{ijkl}^{(1)}$, where $x_{\min} = 10^{-4}$, for reasons which will be explained later.

The material type, that is, material phase 1, phase 2 or void, can vary from finite element to finite element as seen in Fig. 1. With a fine finite-element discretization, this allows us to define complicated bimaterial topologies within the design domain. Having discretized the design domain (the periodic base cell) with N finite elements, the design problem consists in assigning either phase 1, 2 or void to each element such that the objective function is minimized.

Even for a small number of elements, this integer-type optimization problem becomes a huge combinatorial problem that is impossible to solve. For a small design problem with $N = 100$, the number of different distributions of the three material phases would be astronomical ($3^{100} = 5 \cdot 10^{47}$). As each function evaluation requires a full finite element analysis, it is hopeless to solve the optimization problem using random search methods such as, genetic algorithms or simulated annealing methods, which use a large number of function evaluations and do not make use of sensitivity information. Following the idea of standard topology optimization procedures, the problem is therefore relaxed by allowing the material at a given point to be a mixture of the three phases. This makes it possible to find sensitivities with respect to design changes, which in turn allows us to use mathematical programming methods to solve

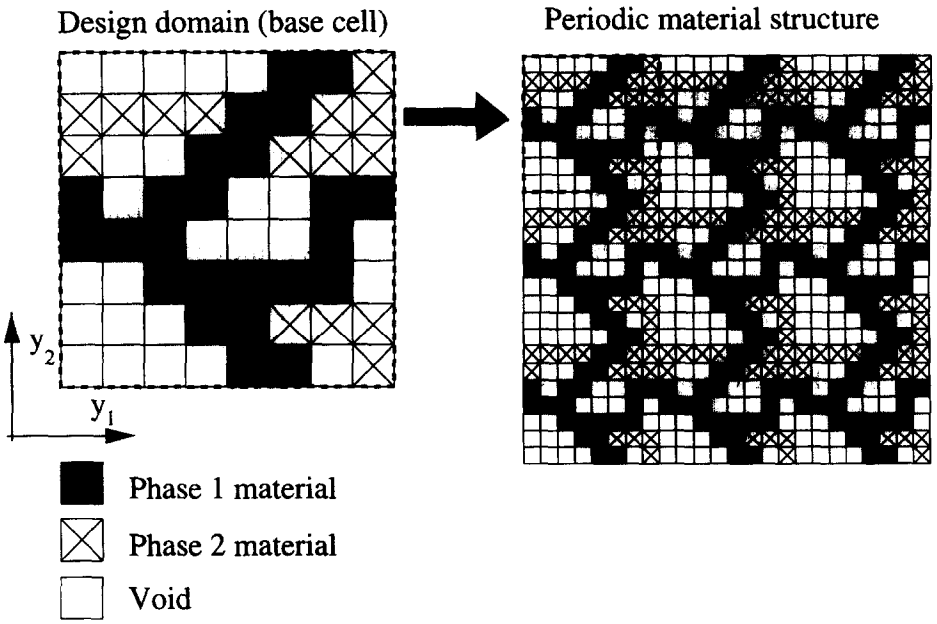

Fig. 1. Design domain and discretization for the three-phase topology optimization problem. Each square represents one finite element which can consist of either phase 1 or 2 material or void.

the optimization problem. At the end of the optimization procedure however, we hope to have a design where each element is either void, phase 1 or phase 2 material.

Using a simple artificial mixture assumption, the local stiffness and thermal strain coefficient tensors in element e can be written as a function of the two design variables x_1^e and x_2^e

$$C_{ijkl}^e(x_1^e, x_2^e) = (x_1^e)^\eta[(1-x_2^e)C_{ijkl}^{(1)} + x_2^e C_{ijkl}^{(2)}],$$
$$\alpha_{ij}^e(x_2^e) = (1-x_2^e)\alpha_{ij}^{(1)} + x_2^e \alpha_{ij}^{(2)}, \tag{4}$$

where η is a penalization factor discussed later. The variable $x_1^e \in [x_{\min}, 1]$ can be seen as a local density variable with $x_1^e = x_{\min}$ meaning that the given element is "void" and $x_1^e = 1$ meaning that the given element is solid material. The variable $x_2^e \in [0, 1]$ is a "mixture coefficient" with $x_2^e = 0$ meaning that the given element is pure phase 1 material and $x_2^e = 1$ meaning that it is pure phase 2 material. The local thermal strain tensor $\alpha_{ij}^e(x_2^e)$ is not dependent on the density variable x_1^e. This can be explained by the fact that once we have chosen the local material mixture (i.e. the value of x_2^e), the thermal strain coefficient does not change with density.

It should be emphasized that the local material assumptions (4) only are valid for the design variables taking the extreme values.† Nevertheless, during the design process we allow intermediate values meaning that we are working with artificial

† A material with constitutive behavior close to that described could be realized as an isotropic porous triangular microstructure (Díaz *et al.*, 1997).

(non-existing) materials. This violation is not critical as long as we end up with a discrete design as discussed in the introduction.

Experience shows that the penalty parameter η should be given values ranging from 3 to 10 depending on the design problem. The influence of the penalty parameter can be explained as follows: let us assume that $x_2^e = 0$ in element e. The local stiffness tensors dependence of x_1^e (4) can then be written as $C_{ijkl}^e(x_1^e) = (x_1^e)^\eta C_{(ijkl)}^{(1)}$. By specifying a value of η higher than one, the local stiffness for fixed $x_1^e < 1$ is lowered, thus making it "uneconomical" to have intermediate densities in the optimal design.

Constraints on volume fractions. Having defined the design variables x_1 and x_2 above, and assuming that the design domain has been discretized by N finite elements of volume Y^e, the volume fractions of the three phases can be calculated as the sums

$$c^{(1)} = \frac{1}{Y}\sum_{e=1}^{N} x_1^e(1-x_2^e)\,Y^e, \quad c^{(2)} = \frac{1}{Y}\sum_{e=1}^{N} x_1^e x_2^e\,Y^e, \quad c^{(0)} = 1-c^{(1)}-c^{(2)}, \tag{5}$$

where Y is the volume of the base cell. For a specific design problem, we might want to constrain the volume fractions of the phases. This can be done by defining two volume fraction constraints as

$$c_{\min}^{(1)} \leqslant c^{(1)} \leqslant c_{\max}^{(1)}, \quad c_{\min}^{(2)} \leqslant c^{(2)} \leqslant c_{\max}^{(2)}, \tag{6}$$

where $c_{\min}^{(1)}$, $c_{\min}^{(2)}$, $c_{\max}^{(1)}$ and $c_{\max}^{(2)}$ are lower and upper bounds on the volume fractions of material 1 and 2, respectively. By setting the lower bound constraint equal to the upper bound constraint, it is possible to fix the volume fractions of the individual phase.

Isotropy or square symmetry constraints. For the purpose of designing materials with either orthotropic, square symmetric or isotropic elastic parameters, such constraints must be implemented in the optimization problem. Orthotropy of the materials can be obtained simply by specifying at least one geometrical symmetry axis in the base cell. Assuming that a material structure is orthotropic, the condition for square symmetry of the elasticity tensor is that $C_{1111}^{(*)} - C_{2222}^{(*)} = 0$, and the conditions for isotropy of the elasticity tensor under plane stress assumption are that $C_{1111}^{(*)} - C_{2222}^{(*)} = 0$ and $(C_{1111}^{(*)} + C_{2222}^{(*)}) - 2(C_{1122}^{(*)} + 2C_{1212}^{(*)}) = 0$. Finally, the condition for thermal expansion isotropy is that $\alpha_{11}^{(*)} - \alpha_{22}^{(*)} = 0$ and $\alpha_{12}^{(*)} = 0$. These conditions are difficult to implement as equality constraints in an optimization problem because the starting guess might be infeasible (i.e. anisotropic). Therefore, it is chosen to implement the constraints as a penalty function added to the cost function. The penalty function is defined as the squared error in obtaining either square symmetry, elastic or thermal isotropy, times the penalization factors r_1, r_2 and r_3, respectively. It should be noted here that three 60° symmetry lines of a microstructure is a sufficient but not a necessary condition for isotropy. Indeed, this paper shows examples of isotropic material structures with only one line of symmetry.

The errors in obtaining square symmetry or isotropy, respectively, can be written as

$$\text{Error}_{\text{sq}} = \frac{(C^{(*)}_{1111} - C^{(*)}_{2222})^2}{(C^{(*)}_{1111} + C^{(*)}_{2222})^2},$$

$$\text{Error}_{\text{iso}} = \frac{[(C^{(*)}_{1111} + C^{(*)}_{2222}) - 2(C^{(*)}_{1122} + 2C^{(*)}_{1212})]^2}{(C^{(*)}_{1111} + C^{(*)}_{2222})^2} + \text{Error}_{\text{sq}}. \tag{7}$$

Expressions similar to Error_{sq} and $\text{Error}_{\text{iso}}$ are also known in the literature of composite materials (e.g. Christensen, 1979) as the practical composite parameters U_2 and U_3.

The error in obtaining isotropic thermal expansion can be defined as

$$\text{Error}_{\text{therm}} = \frac{(\alpha^{(*)}_{12})^2 + (\alpha^{(*)}_{11} - \alpha^{(*)}_{22})^2}{(\alpha^{(*)}_{11} + \alpha^{(*)}_{22})^2}. \tag{8}$$

Lower bound constraints on effective stiffness. As will be seen later, extreme thermal properties can be obtained if we allow the overall stiffness of the material to be small. Low stiffness is generally undesirable and therefore we will introduce a lower bound constraint on the directional Young's moduli $E^{(*)}_1$ and $E^{(*)}_2$ or on the bulk modulus $k^{(*)}$ of the material.

Such constraints can be written as $g_{i(\min)} \leqslant g_i(C^{(*)}_{ijkl})$. For isotropic materials, we have a lower bound constraint on the bulk modulus $[k^{(*)}_{\min} \leqslant k^{(*)} = ((C^{(*)}_{1111} + C^{(*)}_{2222})/2 + C^{(*)}_{1122})/2]$. For anisotropic materials, we might want to constrain the value of the horizontal or vertical Young's moduli, i.e. $[E^{(*)}_{\min(1)} \leqslant E^{(*)}_1 = C^{(*)}_{1111} - (C^{(*)}_{1122})^2/C^{(*)}_{2222}]$ or $[E^{(*)}_{\min(2)} \leqslant E^{(*)}_2 = C^{(*)}_{2222} - (C^{(*)}_{1122})^2/C^{(*)}_{1111}]$.

Lower bound constraints on design variables. For computational reasons (singularity of the stiffness matrix in the finite element formulation), the lower bound on design variable x^e_1 is set to $x_{\min}$; not zero ($x_{\min} = 10^{-4}$). Numerical experiments show that the "void" regions have practically no structural significance and can be regarded as real void regions. The bounds on the design variables can thus be written as $0 < x_{\min} \leqslant x^e_1 \leqslant 1$ and $0 \leqslant x^e_2 \leqslant 1$.

The final optimization problem. An optimization problem including above mentioned features can now be written as

$$\begin{aligned}
&\text{Minimize}: \Phi(\mathbf{x}_1, \mathbf{x}_2) = f(\alpha^{(*)}_{ij}, \beta^{(*)}_{ij}) + r_1\,\text{Error}_{\text{sqr}} + r_2\,\text{Error}_{\text{iso}} + r_3\,\text{Error}_{\text{therm}};\\
&\text{subject to}: g_{i(\min)} \leqslant g_i(C^{(*)}_{ijkl}), \quad i = 1, \ldots, M;\\
&\qquad c^{(1)}_{\min} \leqslant c^{(1)} \leqslant c^{(1)}_{\max};\\
&\qquad c^{(2)}_{\min} \leqslant c^{(2)} \leqslant c^{(2)}_{\max};\\
&\qquad \mathbf{0} < \mathbf{x}_{\min} \leqslant \mathbf{x}_1 \leqslant \mathbf{1};\\
&\qquad \mathbf{0} \leqslant \mathbf{x}_2 \leqslant \mathbf{1},
\end{aligned} \tag{9}$$

where $\mathbf{x}_1$ and $\mathbf{x}_2$ are the N-vectors containing the design variables and the three penalty parameters r_i can be set to zero or non-zero values, depending on the design isotropy type.

2.2. *Sequential linear programming method*

Topology optimization problems in the literature often consist in the optimization of a simple energy functional (e.g. compliance or eigenfrequencies) with a single constraint on material resource, and these problems can therefore be solved very efficiently using optimality criteria methods. In this paper, however, we are considering several different objective functions and multiple constraints which can not be written in energy forms and therefore it will be cumbersome if not impossible to formulate the optimization problem as an optimality criteria problem. Instead we will use a mathematical programing method called sequential linear programming (SLP), which consists in the sequential solving of an approximate linear subproblem, obtained by writing linear Taylor series expansions for the objective and constraint functions. The SLP method was successfully used in optimization of truss structures by Pedersen (1970) and was evaluated as a robust, efficient and easy to use optimization algorithm in a review paper by Schittkowski (1994).

Using the sequential linear programing method, the optimization problem (9) is solved iteratively. In each iteration step, the optimization problem is linearized around the current design point $\{\mathbf{x}_1, \mathbf{x}_2\}$ using the first part of a Taylor series expansion and the vector of optimal design changes $\{\Delta\mathbf{x}_1, \Delta\mathbf{x}_2\}$ is found by solving the linear programming problem

$$\text{Minimize}: \Phi + \left\{\frac{\partial\Phi}{\partial\mathbf{x}_1}, \frac{\partial\Phi}{\partial\mathbf{x}_2}\right\}^{\mathrm{T}} \{\Delta\mathbf{x}_1, \Delta\mathbf{x}_2\};$$

$$\text{subject to}: g_{i(\min)} - g_i \leqslant \left\{\frac{\partial g}{\partial\mathbf{x}_1}, \frac{\partial g}{\partial\mathbf{x}_2}\right\}^{\mathrm{T}} \{\Delta\mathbf{x}_1, \Delta\mathbf{x}_2\}, \quad i = 1, \ldots, M,$$

$$c^{(1)}_{\min} - c^{(1)} \leqslant \left\{\frac{\partial c^{(1)}}{\partial\mathbf{x}_1}, \frac{\partial c^{(1)}}{\partial\mathbf{x}_2}\right\}^{\mathrm{T}} \{\Delta\mathbf{x}_1, \Delta\mathbf{x}_2\} \leqslant c^{(1)}_{\max} - c^{(1)},$$

$$c_{2\min} - c^{(2)} \leqslant \left\{\frac{\partial c^{(2)}}{\partial\mathbf{x}_1}, \frac{\partial c^{(2)}}{\partial\mathbf{x}_2}\right\}^{\mathrm{T}} \{\Delta\mathbf{x}_1, \Delta\mathbf{x}_2\} \leqslant c_{2\max} - c^{(2)},$$

$$\{\Delta\mathbf{x}_{1L}, \Delta\mathbf{x}_{2L}\} \leqslant \{\Delta\mathbf{x}_1, \Delta\mathbf{x}_2\} \leqslant \{\Delta\mathbf{x}_{1U}, \Delta\mathbf{x}_{2U}\}, \tag{10}$$

where $\Delta\mathbf{x}_{1L}$, $\Delta\mathbf{x}_{2L}$, $\Delta\mathbf{x}_{1U}$ and $\Delta\mathbf{x}_{2U}$ are move-limits on the design variables. The move-limits are adjusted for the absolute limits given in (9).

The applied move-limit strategy is important for the stable convergence of the algorithm. Here we use the simple rule that the move-limit for a specific design variable is increased by a factor of 1.4 if the change in the design variable has the same sign for two subsequent steps. Similarly the move-limit is decreased by a factor of 0.6 if the change in the design variable has opposite signs for two subsequent steps.

The sensitivities, which are necessary to solve the linearized sub-problem (10), are derived in Appendix B, and are calculated locally for each element. The appendix also shows that no additional finite-element problems have to be solved to find the sensitivities needed.

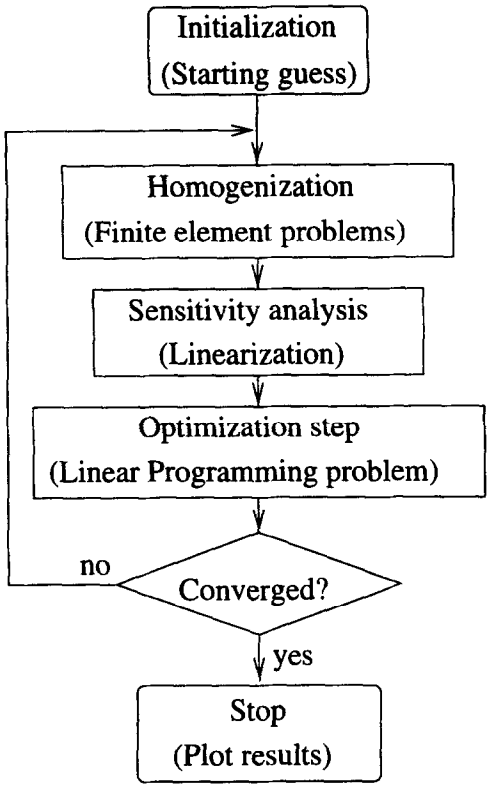

Fig. 2. Flowchart of the design algorithm.

2.3. *Numerical implementation issues*

This section describes the numerical implementation of the three-phase topology optimization problem including the finite-element discretization and procedures, the linear programming package DSPLP (Hanson and Hiebert, 1981) from the SLATEC library, control of move-limits and a flowchart of the procedure.

A flowchart of the design algorithm is shown in Fig. 2. The individual steps of the design procedure are described in the following.

Initialization. First, we initialize the design problem by selecting the objective function, specifying a lower bound on the stiffness, selecting isotropy type and symmetry lines. We also choose the design domain discretization, using 900 or 3600 four-node linear displacement finite elements, corresponding to 30 by 30 or 60 by 60 element discretizations, depending on accuracy demands and available computing time. To save computer time, a design problem can first be solved on a 30 by 30 element mesh. When a solution has been reached, each of the elements are divided into four and the procedure is continued until convergence.

Starting guess. Starting distribution of densities and material types (i.e. starting values of the design variable vectors $\mathbf{x}_1$ and $\mathbf{x}_2$) is up to the user. Having absolutely no idea of what the solution will look like, a random distribution of densities and

material types is chosen as the starting guess. If the user has an idea of what the solution will look like or he has an old solution to a similar problem, a considerable amount of computing time is saved by using this (old) topology as a starting guess.

Homogenization step. The equilibrium equations (A.2) for the homogenization problem derived in Appendix A, are solved using the finite-element method applied to calculation of effective material properties in Bourgat (1977) and Guedes and Kikuchi (1991).

Sensitivity analysis. The sensitivity analysis necessary to solve the linear programming problem in (10) is derived in Appendix B. The computation of the sensitivities is fast because they can be found from the strain fields already computed by the homogenization procedure.

Linear programming problem. The linear programming problem (10) is solved using a linear programming solver DSPLP (Hanson and Hiebert, 1981) from the SLATEC library. As the optimization is non-sparse, the DSPLP routine is invoked with an option for no sparsity. Nevertheless, the routine has proven faster and demands less storage space than other LP-algorithms tests.

Convergence. The iterative design procedure is repeated until the change in each design variable from step to step is lower than 10^{-4} (by experience).

2.4. *Problems related to topology optimization*

This section discusses some numerical difficulties due to the finite-element discretization, namely checkerboard patterns, mesh-dependencies and local minima.

The checkerboard and mesh-dependency problems. Applying the topology optimization method to different design problems, one often encounters regions of alternating solid and void elements, referred to as checkerboards, in the "optimal solutions". The regions are seen in many works on general topology optimization and it was earlier believed, that such regions represented optimal microstructure on the finite-element level. However, two recent papers by Jog and Haber (1996) and Díaz and Sigmund (1995) conclude, that regions with checkerboard patterns have artificially high (numerical) stiffness (higher than the theoretical bounds) and can be explained by poor numerical modeling of the stiffness of checkerboards by lower order finite elements. Both papers conclude, that checkerboards are certainly prone to appear in topology optimization using four-node finite elements, as here, but also using higher order elements such as nine-node quadratic displacement finite elements.

Another problem, due to the finite-element discretization, is mesh dependency, which refers to the non-convergence of solutions with mesh refinement. Refining the finite-element mesh should ideally result in the same topology as for a coarse mesh but with better definitions of the boundaries between the material phases. However, a refinement does result in a solution with a more complicated (finer) microstructure. Methods to avoid this problem have been suggested in three recent papers. Haber *et al.* (1996) suggest the introduction of a constraint on global perimeter. In a paper on bone remodeling, closely related to topology optimization methods, Mullender *et al.* (1994) suggest a mesh-independency algorithm that assumes that bone growth at a

point is dependent on the loads in a (mesh-dependent) neighborhood of the point. A method related to the latter approach, but with different origin, is proposed in Sigmund (1994a), who performs the density update based on low-pass filtered strain energy fields. To avoid the checkerboard and mesh-dependency problems, we use the method suggested in Sigmund (1994a).

Local minima. The topology optimization problem is very prone to converge to local minima. However, introducing the mesh-independency algorithm (Sigmund, 1994a) makes it possible to prevent this problem to a certain extent. Solving a cell design problem is typically done as follows. First we solve the optimization problem with a low value of the low-pass filter parameter, i.e. we do not allow rapid variation in the element densities. This results in a design with large areas of intermediate densities but it also prevents the design in converging to a local minimum (binary design). Gradually, we increase the low-pass filter parameter, in turn letting the design problem converge. In that way, we gradually arrive at a solution which is entirely binary and which is, hopefully, a global optimum. To make sure that the actually obtained microstructures are global optima indeed, the same optimization problem is always solved using differing starting guesses, move-limit strategies and choices of low-pass filter parameter and penalty parameter η. However, as will be seen later, topologically different solutions with similar values of the objective function have been found when solving specific design problems. Solutions which are "shifted" (translated half a base cell dimension) of other solutions have also been encountered. The fact that the effective properties of the design examples are close to theoretical bounds supports our belief, that we are finding the optimal topologies with the proposed design procedure.

Computing time. One design iteration, typically takes 3 s (30 by 30 element discretization) and 20 s (60 by 60 element discretization) on an Indigo 2 work station. To arrive at an optimal solution, depending on starting guess, several thousand iterations are needed. Including interaction by the user, a full design process may take two working days. Comparing the computing time and the number of iterations with other works in topology optimization it can be concluded that the present procedure is extremely slow. However, these other works in topology optimization usually consider self-adjoint loading problems and statically determinant structures where a solution can be found often within a few design iterations. This is due to the fact that the stress fields of statically determinate structures do not change much with design. In this paper, however, the optimal strain and stress fields for the given design problem are unknown in the beginning and must emerge gradually during the design process together with the optimal material distribution.

3. RIGOROUS EXPRESSIONS AND BOUNDS ON EFFECTIVE THERMOELASTIC PROPERTIES

Rigorous expressions for the effective thermal expansion coefficients of two-phase, *isotropic* composites and rigorous bounds on the effective coefficients of three-phase, *isotropic* composites will serve to benchmark the design algorithm. For simplicity, we

assume that the constituent phases are isotropic which implies that they can be described by their Young's moduli $E^{(0)}$, $E^{(1)}$, and $E^{(2)}$, their Poisson's ratios $\nu^{(0)}$, $\nu^{(1)}$ and $\nu^{(2)}$ and their thermal strain coefficients $\alpha^{(0)}$, $\alpha^{(1)}$ and $\alpha^{(2)}$. It is also assumed that the composite is macroscopically isotropic. The bulk and shear moduli of the phases are then

$$k^{(i)} = \frac{E^{(i)}}{2(1-\nu^{(i)})}, \quad \mu^{(i)} = \frac{E^{(i)}}{2(1+\nu^{(i)})}, \quad i = 0, 1, 2. \tag{11}$$

3.1. *Two-phase materials*

The effective thermal strain coefficient $\alpha^{(*)}$ of a two-phase isotropic material is explicitly given in terms of the effective bulk modulus $k^{(*)}$ (Levin, 1967; Rosen and Hashin, 1970)

$$\alpha^{(*)} = \frac{\alpha^{(1)}k^{(1)}(k^{(2)}-k^{(*)}) - \alpha^{(2)}k^{(2)}(k^{(1)}-k^{(*)})}{k^{(*)}(k^{(2)}-k^{(1)})}. \tag{12}$$

The best bounds on the isotropic effective bulk modulus $k^{(*)}$, given volume fraction information only, were derived by Hashin and Shtrikman (1963) and read

$$\left(\overline{\left(\frac{1}{k+\mu_{\min}}\right)}\right)^{-1} - \mu_{\min} \leqslant k^{(*)} \leqslant \left(\overline{\left(\frac{1}{k+\mu_{\max}}\right)}\right)^{-1} - \mu_{\max}, \tag{13}$$

where bars denote averaged values and $\mu_{\min}$ and $\mu_{\max}$ are the minimum and maximum shear moduli (11) of the two phases, respectively [(13) is also valid for multiple phases]. Bounds for the thermal strain coefficient are therefore obtained by inserting the upper and lower bounds for the bulk modulus (13) into (12).

3.2. *Three-phase materials*

Bounds on the effective thermal strain coefficient $\alpha^{(L)} \leqslant \alpha^{(*)} \leqslant \alpha^{(U)}$ of three-phase, isotropic composites were found by Schapery (1968) and Rosen and Hashin (1970) and read

$$\left.\begin{matrix}\alpha^{(U)} \\ \alpha^{(L)}\end{matrix}\right\} = \frac{1}{\overline{(1/k)} - 1/\bar{k}} \left\{ \bar{\alpha}\left(\overline{\frac{1}{k^{(*)}}} - \frac{1}{\bar{k}}\right) + \frac{\overline{k\alpha}}{\bar{k}}\left(\overline{\left(\frac{1}{k}\right)} - \frac{1}{k^{(*)}}\right) \right.$$
$$\left. \pm \Psi \left(\overline{\left(\frac{1}{k}\right)} - \frac{1}{k^{(*)}}\right)^{1/2} \left(\frac{1}{k^{(*)}} - \frac{1}{\bar{k}}\right)^{1/2} \right\}, \tag{14}$$

where

$$\Psi = \left\{ \left(\overline{\left(\frac{1}{k}\right)} - \frac{1}{\bar{k}}\right)\left(\overline{(ka^2)} - \frac{\overline{(ka)^2}}{\bar{k}}\right) - \left(\bar{a} - \frac{\overline{(ka)}}{k}\right)^2 \right\}^{1/2}.$$

Note that there is a typographical error in the equation (14) in Rosen and Hashin (1970) as well as in the corresponding formula in the text by Christensen (1979).

A bounded domain of possible effective bulk moduli and thermal strain coefficients

for a specific choice of constituent phases is shown in Fig. 4. We found that the proposed design method did not yield pairs $(k^{(*)}, \alpha^{(*)})$ that were close to the Schapery–Rosen–Hashin bounds (14). There were two possible explanations for this discrepancy: either the design method could not find the optimal solutions, or the bounds themselves could be improved upon. Indeed, the latter explanation turned out to be true.

Inspired by the above mentioned discrepancy Gibiansky and Torquato (1997) recently found improved bounds, which are also shown in Fig. 4. The new bounds can be written as

$$\left.\begin{matrix}\alpha^{(U)}\\ \alpha^{(L)}\end{matrix}\right\} = \frac{1}{k^{(*)}(k^{(U)}-k^{(L)})}\left\{(k^{(U)}-k^{(*)})(k^{(L)}+\mu_{\min})\overline{\left(\frac{k\alpha}{k+\mu_{\min}}\right)}\right.$$
$$\left. + (k^{(*)}-k^{(L)})(k^{(U)}+\mu_{\max})\overline{\left(\frac{k\alpha}{k+\mu_{\max}}\right)} \pm \Psi^{1/2}(k^{(U)}-k^{(*)})^{1/2}(k^{(*)}-k^{(L)})^{1/2}\right\},$$

where

$$\Psi = -(k^{(U)}+\mu_{\max})(k^{(L)}+\mu_{\min})\left\{\overline{\left(\frac{k\alpha}{k+\mu_{\min}}\right)} - \overline{\left(\frac{k\alpha}{k+\mu_{\max}}\right)}\right\}^2$$
$$+ (\mu_{\max}-\mu_{\min})\left\{(k^{(L)}+\mu_{\min})\overline{\left(\frac{k\alpha}{k+\mu_{\min}}\right)}^2 - (k^{(U)}+\mu_{\max})\overline{\left(\frac{k\alpha}{k+\mu_{\max}}\right)}^2\right\}$$
$$+ (k^{(U)}-k^{(L)})\left\{\overline{\left(\frac{k^2\alpha^2}{k+\mu_{\min}}\right)} + \mu_{\max}\overline{\left(\frac{k\alpha^2}{k+\mu_{\max}}\right)} - \overline{k\alpha^2}\right\},$$

and $k^{(L)}$ and $k^{(U)}$ are the lower and upper Hashin–Shtrikman bounds on bulk modulus as given in (13). As will be seen in the subsequent section, the solutions obtained by the design procedure are very close to the new bounds.

Examination of the thermoelastic bounds in Fig. 4 reveals that the extreme values (e.g. negative values) of thermal strain coefficients only are possible for low bulk moduli. If we simply tried to minimize/maximize the thermal strain $\alpha^{(*)}$, we would end up with a very weak material. Therefore, there is a tradeoff between extremizing thermal strain coefficients on the one hand and ending up with a stiff material on the other. This problem will be discussed in more detail in the next section.

4. DESIGN EXAMPLES

In this section, we will first discuss design examples with mixtures of hypothetical materials. These examples are used to benchmark the design algorithm for two- and three-phase design. We will also study other design examples that utilize real materials as constituent phases.

During the iterative procedure, a postscript plot of the topology is generated every 10 iterations. The plot shows the current density and material distribution in the base

cell, thus allowing the user to follow the evolution of the microstructure and interact if necessary. The plots in the following sections show the optimal density and material type distributions for the different design problems. If an element is dominating material phase 2 (i.e. $x_2^e > 0.5$), the element is illustrated by a cross with gray scale denoting the density x_1^e; white means void ($x_1^e = x_{\min}$) and black means solid ($x_1^e = 1$). If the element is dominating material phase 1 (i.e. $x_2^e < 0.5$), it is shown as a filled rectangle with gray values interpreted as before. For all examples, we both show the resulting topologies represented by a single base cell (the design domain) and as a repeated microstructure consisting of 3 by 3 base cells.

4.1. *Comparison with two-phase bounds*

The two-phase bounds given by (12) and (13) are used for benchmarking the design algorithm for two-phase design. The non-dimensionalized material data for the two phases are chosen as $E^{(2)}/E^{(1)} = 10$, $\nu^{(1)} = \nu^{(2)} = 0.3$, $\alpha^{(2)}/\alpha^{(1)} = 10$ and $c^{(1)} = c^{(2)} = 0.5$.

The bounds on the thermal strain coefficient for this mixture are found from (12) to be given by $6.3412 \leqslant \alpha^{(*)}/\alpha^{(1)} \leqslant 8.2524$ and the bounds on the bulk modulus are found from (13) to be given by $2.1465 \leqslant k^{(*)}/k^{(1)} \leqslant 3.6396$.

First we try to maximize the effective thermal strain coefficient which through (12) corresponds to maximizing the effective bulk modulus. Specifying macroscopic isotropy and horizontal and vertical geometric symmetry, the attained values with a 60 by 60 element discretization are $\alpha^{(*)}_{\max}/\alpha^{(1)} = 8.2349$ and $k^{(*)}_{\max}/k^{(1)} = 3.6181$. If we try to minimize the thermal strain coefficient we just get the "inverted" microstructure, meaning that the two domains are interchanged. The actual numbers obtained for this case are $\alpha^{(*)}_{\min}/\alpha^{(1)} = 6.3907$ and $k^{(*)}_{\min}/k^{(1)} = 2.1702$. The optimal topology of the microstructure for maximum thermal strain value and isotropy constraint is shown in Fig. 3 (top).

Relaxing the isotropy requirement by only specifying square symmetry (but still specifying horizontal and vertical geometric symmetry), the attained values with a 60 by 60 element discretization are $\alpha^{(*)}_{\max}/\alpha^{(1)} = 8.2320$ and $k^{(*)}_{\max}/k^{(1)} = 3.6116$, $\alpha^{(*)}_{\min}/\alpha^{(1)} = 6.3733$ and $k^{(*)}_{\min}/k^{(1)} = 2.1637$, respectively. The actual topology of the optimal two-phase microstructure is shown in Fig. 3 (bottom). As expected, the optimal microstructural topologies resemble the energy minimizing microstructures of Vigdergauz (1989).

It should be noted that we get the same (except for numerical errors) effective properties for the isotropic material and square symmetric microstructures. This means, that the optimal rigidity Vigdergauz microstructures can be made isotropic by using the new geometry in Fig. 3 (top) instead of the one in Fig. 3 (bottom). Not surprisingly, it also shows that solutions with widely different topologies can have the same values of the objective function.

4.2. *Comparison with three-phase bounds*

The three-phase bounds given by (13)–(15) are used for benchmarking the design algorithm for three-phase design. The material data for the two phases are chosen as $E^{(1)}/E^{(2)} = 1$, $\nu^{(1)} = \nu^{(2)} = 0.3$, $\alpha^{(2)}/\alpha^{(1)} = 10$, and the volume fractions are prescribed to be $c^{(1)} = c^{(2)} = 0.25$ (i.e. $c^{(0)} = 0.5$). Note that the volume fractions c_i are held fixed

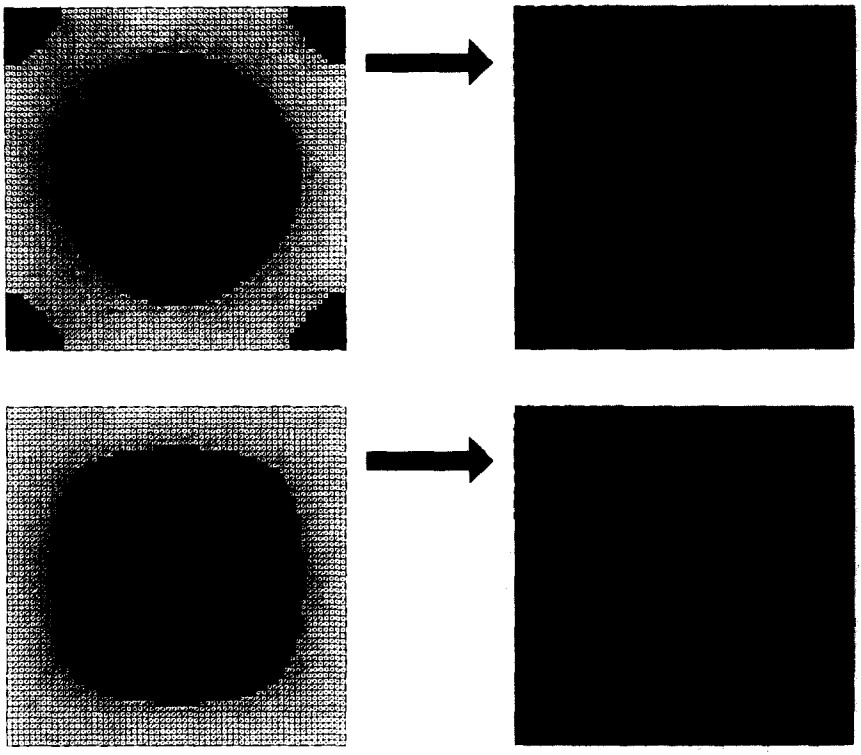

Fig. 3. Optimal microstructures for two-phase design problem. Maximization of thermal strain coefficient with and without macroscopic isotropy constraint (top and bottom, respectively). The filled regions consist of low expansion material (phase 1) and the cross-hatched regions consist of high expansion material (phase 2).

for this hypothetical composite, to allow for comparison with the bounds and for easy interpretation of the results.

Four three-phase design examples, constrained to be elastically isotropic, are considered as follows.

(a) Minimization of the *isotropic* thermal strain coefficient $\alpha^{(*)}/\alpha^{(1)}$ with a lower bound constraint on the effective bulk modulus given as 10% of the theoretically attainable bulk modulus, i.e. $k^{(*)}/k^{(1)} = 0.0258$. Horizontal geometric symmetry is specified.

(b) Same as design example (a) but with horizontal, vertical and diagonal (geometric) symmetry.

(c) Maximization of bulk modulus $k^{(*)}/k^{(1)}$ for fixed zero thermal expansion $\alpha^{(*)}/\alpha^{(1)} = 0$. Horizontal geometric symmetry is specified.

(d) Maximization of isotropic thermal stress coefficient $\beta^{(*)}/\beta^{(1)}$ with horizontal, vertical and diagonal geometric symmetry.

The old and new theoretical bounds are given by (13) and (15), respectively, and they are shown in Fig. 4. In examples (a) and (b), the lower bound on the possible thermal strain coefficient is $-5.567 \leqslant \alpha^{(*)}/\alpha^{(1)}$. In example (c), the upper bound on possible

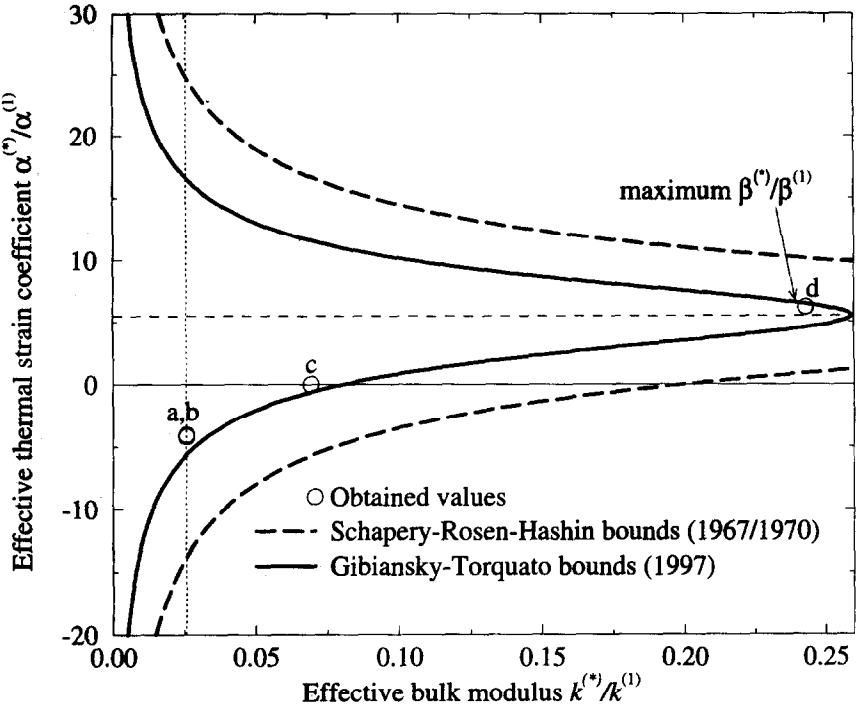

Fig. 4. Bounds for three-phase design example. The circles with letters a–d denote the obtained values for the microstructures shown in Figs 5 and 6.

bulk modulus for zero thermal expansion is $k^{(*)}/k^{(1)} \leqslant 0.0692$. The upper bound on the thermal stress coefficient in design example (d) is $\beta^{(*)}/\beta^{(1)} \leqslant 3.15$ (for $k^{(*)}/k^{(1)} = 0.237$).

The resulting topologies are shown in Figs 5 and 6 and their effective properties are shown in Table 1 and plotted as small circles in Fig. 4. Studying the graph in Fig. 4, we see that the obtained effective values are far away from the original Schapery–Rosen–Hashin bounds. This discrepancy inspired Gibiansky and Torquato to try to improve the bounds and indeed improvement was possible as seen in Fig. 4. The effective values of the examples (a)–(d) are still somewhat away from the improved bounds. This can be explained by the fact that the new bounds by Gibiansky and Torquato have not been proven to be optimal. Furthermore, it is our experience that a finer finite-element mesh makes it possible to get closer to the bounds. In example (a), the minimum thermal strain coefficient obtained for a 30 by 30 mesh is $\alpha^{(*)}/\alpha^{(1)} = -3.59$ and $\alpha^{(*)}/\alpha^{(1)} = -4.17$ for the 60 by 60 element discretization shown in Fig. 5. Due to computer time limitations, it has not been possible to try out finer discretizations.

The actual mechanisms behind the extreme thermal expansion coefficients of the material structures can be difficult to understand. To visualize one of the mechanisms, the (exaggerated) displacements, due to an increase in temperature of the microstructure in Fig. 5 (bottom), is shown in Fig. 7. Studying Fig. 7, we note that there appears to be contact between parts of the microstructure. This contact is only due

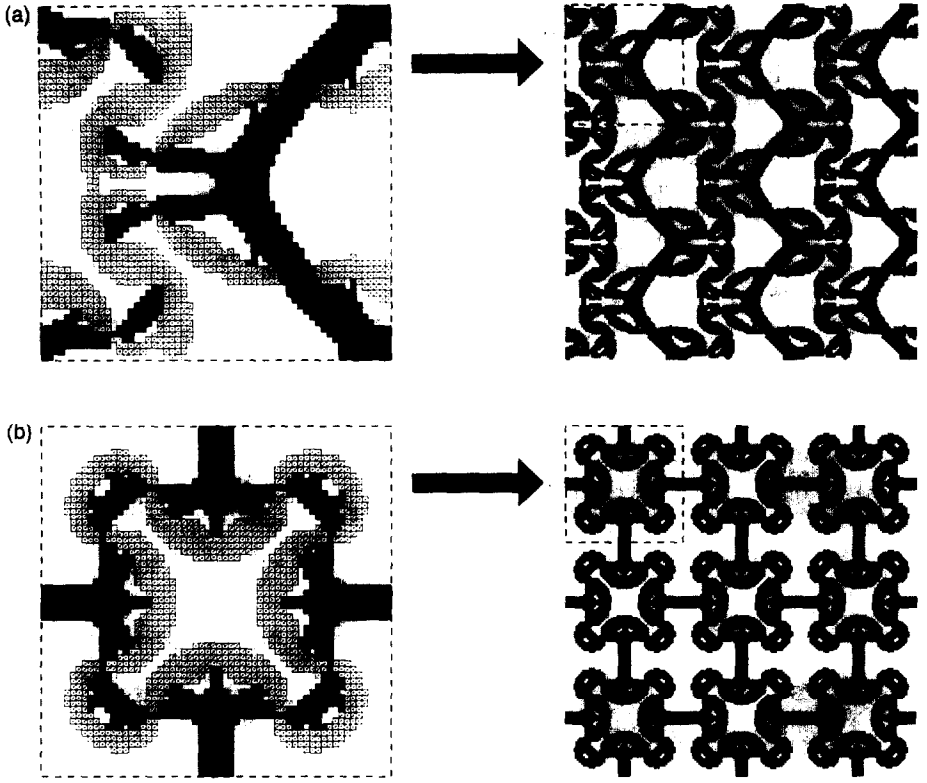

Fig. 5. Examples (a) (top) and (b) (bottom) : optimal microstructures for minimization of effective thermal strain coefficient corresponding to the circles a and b in Fig. 4, respectively. The white regions denote void (phase 0), the filled regions consist of low expansion material (phase 1) and the cross-hatched regions consist of high expansion material (phase 2).

to the magnification of the displacements used in the illustration. The simple linear modeling used here can not take such problems into account. Nevertheless, it would be interesting to extend the analysis to include non-linear behavior including contact, which would open up for a whole new world of interesting design possibilities. We will leave these extensions to future studies.

When allowing low bulk moduli [as in examples (a) and (b)], the main mechanics behind the extreme (negative) thermal expansion is the *reentrant cell structure* having bimaterial components which bend and cause large deformation when heated. The bimaterial interfaces of design examples (a) and (b) bend and make the cell contract, similar to the behavior of negative Poisson's ratio materials (1987). If a higher effective bulk modulus is specified, as in example (c), the intricate bimaterial mechanisms are less pronounced resulting in a less extreme expansion ($\alpha_* = 0$). Finally, maximizing the expansive stress, as in example (d), results in a structure without bimaterial mechanisms, where the high expansion phase (cross hatched phase) is arranged such that it maximizes the horizontal and vertical expansion.

Design examples (a) and (b) in Fig. 5 demonstrate how two, topologically, very different microstructures can have (almost) the same value of the objective function. The only difference between the two examples is the specified geometric symmetry.

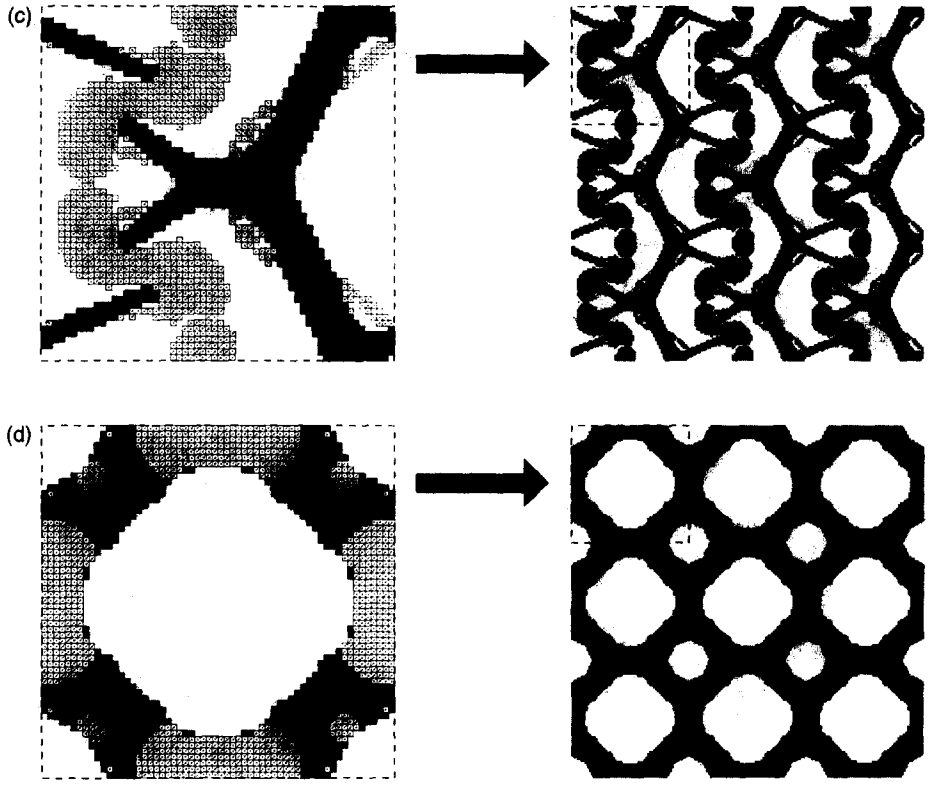

Fig. 6. Examples (c) (top) and (d) (bottom): optimal microstructures for maximization of bulk modulus with zero thermal expansion (top) and maximization of effective thermal stress coefficient (bottom) corresponding to the circles c and d in Fig. 4, respectively. The white regions denote void (phase 0), the filled regions consist of low expansion material (phase 1) and the cross-hatched regions consist of high expansion material (phase 2).

Table 1. *Thermoelastic parameters for optimal three-phase microstructures composed of hypothetical materials compared with the bounds. The white regions denote void, the filled regions consist of low expansion material (phase 1) and the cross-hatched regions consist of high expansion material (phase 2)*

Example	Objective/ constraint	$k^{(*)}/k^{(1)}$ (bound)	$\nu^{(*)}$	$\alpha^{(*)}/\alpha^{(1)}$ (bound)	$\beta^{(*)}/\beta^{(1)}$ (bound)
(a) Fig. 5	Min. $\alpha^{(*)}/\alpha^{(1)}$ $k^{(*)}/k^{(1)} \geqslant 0.0258$	0.0258	0.039	-4.17 (-5.567)	
(b) Fig. 5	Min. $\alpha^{(*)}/\alpha^{(1)}$ $k^{(*)}/k^{(1)} \geqslant 0.0258$	0.0258	0.51	-4.02 (-5.567)	
(c) Fig. 6	Max. $k^{(*)}/k^{(1)}$ $\alpha^{(*)}/\alpha^{(1)} \leqslant 0.0$	0.0692 (0.0814)	0.54	0	
(d) Fig. 6	Max. $\beta^{(*)}/\beta^{(1)}$	0.243	0.51		3.01 (3.15)

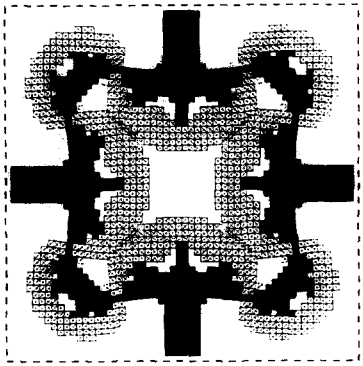

Fig. 7. Thermal displacement of microstructure in Fig. 5 (bottom).

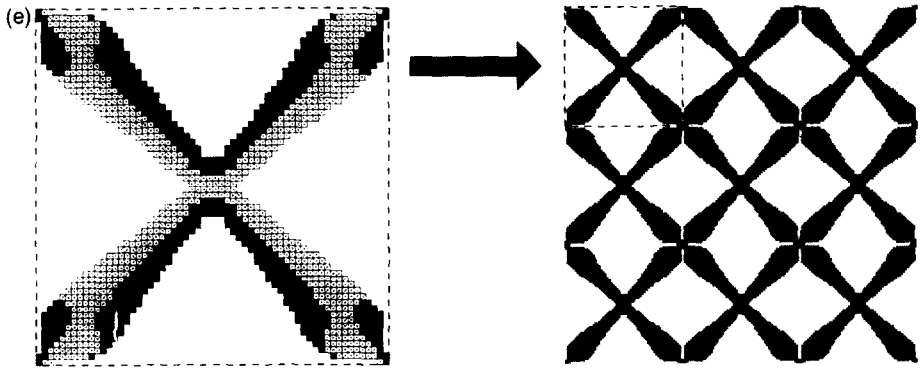

Fig. 8. Example (e): optimal microstructure for maximization of thermal strain in the vertical direction $\alpha_{22}^{(*)}$. The white regions denote void (phase 0), the filled regions consist of low expansion material (phase 1) and the cross-hatched regions consist of high expansion material (phase 2).

In order to check the validity of the effective values computed by the homogenization code, we will make a comparison between a simple example and an idealized beam model. Figure 8 shows the optimal microstructure (e) for maximization of the thermal strain coefficient in the vertical direction $\alpha_{22}^{(*)}/\alpha^{(1)}$. We specify geometrical symmetry about horizontal and vertical axes, effective vertical stiffness component $C_{2222}^{(*)}/C_{2222}^{(1)} \geqslant 0.07$ and volume fractions $c^{(1)}$ and $c^{(2)}$ less than or equal to 0.2. The obtained values are $\alpha_{11}^{(*)}/\alpha^{(1)} = -20.7$ and $\alpha_{22}^{(*)}/\alpha^{(1)} = 33.5$. The actual material volume fractions in the optimal topology are $c^{(1)} = 0.167$ and $c^{(2)} = 0.200$ and effective horizontal and vertical stiffness components are $k^{(*)}/k^{(1)} = 0.070$, respectively.

To check the obtained values, we calculate the effective thermal strain tensor using an idealized beam model in Appendix C. The predicted thermal strain coefficients and bulk modulus, are $\alpha_{11}^{(*)}/\alpha^{(1)} = -21$, $\alpha_{22}^{(*)}/\alpha^{(1)} = 32$ and $k^{(*)}/k^{(1)} = 0.085$, respectively. Good agreement between the idealized beam model and the effective properties is observed.

4.3. *Mixtures of real materials*

For the design of new materials with extreme thermal expansion coefficients, the two base materials should be of equal stiffness but widely differing thermal strain

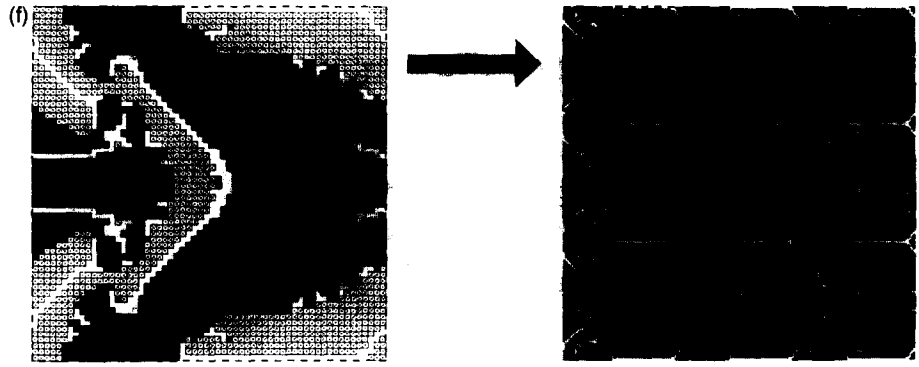

Fig. 9. Example (f): optimal microstructure for minimization of the isotropic thermal stress coefficient $\beta^{(*)}$. The white regions denote void (phase 0), the filled regions consist of Invar (phase 1) and the cross-hatched regions consist of Nickel (phase 2).

coefficients. Two materials fulfilling this requirement are isotropic Invar (Fe–36%Ni) and nickel as discussed in the introduction. For the next design examples, the volume fractions of the material phases are unconstrained. This will allow for a wider range of minimum and maximum values, in contrast to the hypothetical examples (a)–(e) in which the volume fractions were fixed.

The material properties of Invar and nickel can be found in the ASM-Handbook (1993). The Young's moduli are 150 and 200 GPa, respectively, Poisson's ratios are 0.31 for both, and the thermal expansion coefficients are 0.8 μm/(mK) and 13.4 μm/(mK), respectively.

(f) Minimization of the *isotropic* thermal stress coefficient $\beta^{(*)}$. Horizontal geometric symmetry is specified.
(g) Minimization of the *vertical* thermal stress coefficient $\beta_{22}^{(*)}$. Horizontal and vertical symmetry is specified.
(h) Minimization of the *vertical* thermal stress $E_2^{(*)}\alpha_{22}^{(*)}$. Horizontal and vertical symmetry is specified.
(i) Maximization of the *vertical* strain $(\alpha_*)_{22}$ with constrain on vertical Young's modulus $E_2^{(*)} \geqslant 5$ GPa. Horizontal and vertical symmetry is specified.

The resulting topologies are shown in Figs 9, 10 and 11, and their effective properties are shown in Table 2.

To overcome the positive thermal expansion of other surrounding materials, we seek to maximize the *contraction force*, i.e. minimize the isotropic thermal stress coefficient as in example (f). The obtained *isotropic* contraction stress of example (f) is $\beta^{(*)} = -77.6$ kPa/K. By relaxing the isotropy requirement and allowing orthotropic materials the *directional* contraction stress can be increased. In example (g) we minimize the value of $\beta_{22}^{(*)}$ and get the effective value $\beta_{22}^{(*)} = -210$ kPa/K. Minimizing the value of $\beta_{22}^{(*)}$ gives us a composite which for *fixed boundaries* has high contraction force (remember that the thermal stress coefficient $\beta^{(*)}$ is the stress in a material constrained at the boundaries). If we want to maximize the contraction force for a material with free boundaries, we should minimize the product $(E_*)_2(\alpha_*)_{22}$ as done in example (h). The "free boundary" stress of example (g) is $(E_*)_2(\alpha_*)_{22} = -14$

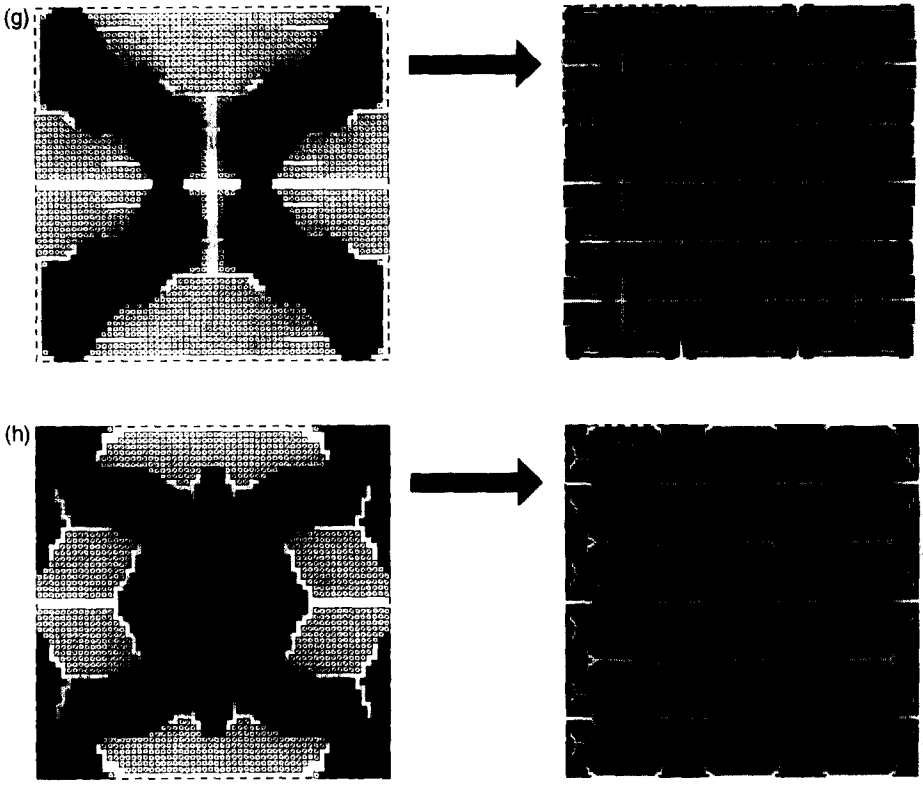

Fig. 10. Examples (g) (top) and (h) (bottom): optimal microstructures for minimization of thermal stress coefficient $\beta_{22}^{(*)}$ (top) and minimization of vertical contraction stress $E_2^{(*)}\alpha_{22}^{(*)}$. The white regions denote void (phase 0), the filled regions consist of Invar (phase 1) and the cross-hatched regions consist of nickel (phase 2).

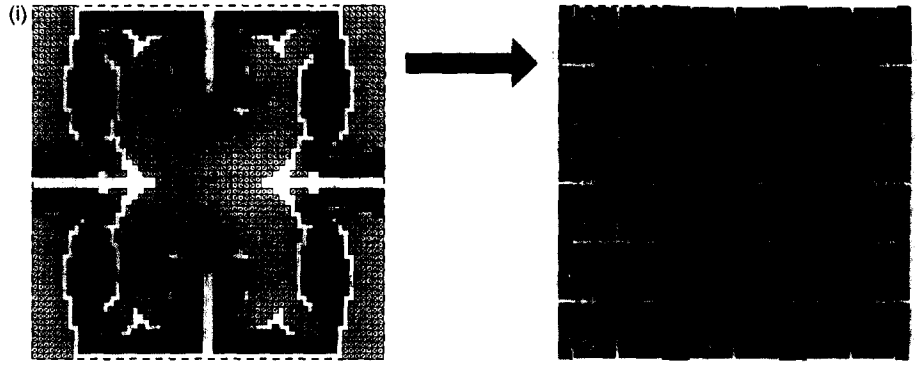

Fig. 11. Example (i): optimal microstructure for maximization of thermal strain in the vertical direction $\alpha_{22}^{(*)}$. The white regions denote void (phase 0), the filled regions consist of Invar (phase 1) and the cross-hatched regions consist of nickel (phase 2).

Table 2. *Thermoelastic parameters for optimal microstructures made of Invar (phase 1) and nickel (phase 2)*

Example	Objective	$\alpha^{(*)}$ $(\alpha_{11}^{(*)}/\alpha_{22}^{(*)})$	$E^{(*)}$ $(E_1^{(*)}/E_2^{(*)})$	$\nu^{(*)}$ $(\nu_{12}^{(*)}/\nu_{21}^{(*)})$	$\beta^{(*)}$ $(\beta_{11}^{(*)}/\beta_{22}^{(*)})$	$c^{(1)}/c^{(2)}$
		μm/(mK)	GPa		kPa/K	
Invar		0.8	150	0.31	174	1/0
Nickel	(Max. $\beta^{(*)}$)	13.4	200	0.31	3884	0/1
(f) Fig. 9	Min. $\beta^{(*)}$	−4.97	14.8	0.055	−77.6	0.60/0.28
(g) Fig. 10	Min. $\beta_{22}^{(*)}$	9.98/−1.59	9.19/8.75	−0.80/−0.76	258/−210	0.49/0.38
(h) Fig. 10	Min. $E_2^{(*)}\alpha_{22}^{(*)}$	5.42/−4.68	69.9/29.5	0.059/0.025	372/−129	0.60/0.30
(i) Fig. 11	Max. $\alpha_{22}^{(*)}$	23.4/35.0	1.09/5.00	−0.14/−0.62	2.01/174	0.38/0.46

kPa/K, whereas the "free boundary" stress of example (h) is $(E_*)_2(\alpha_*)_{22} = -138$ kPa/K.

If we want to *maximize* the expansion stress of the composite, the best choice would be to take solid nickel material both for the isotropic and the directional cases.

The isotropic negative thermal expansion materials in examples (a), (b) and (f) all have positive Poisson's ratios (0.04, 0.52 and 0.055, respectively), showing that there is no mechanistic relationship between negative thermal expansion and negative Poisson's ratio.

In example (i) we see again that allowing orthotropy can lead to high *directional* expansion coefficients. The vertical coefficient $(\alpha_*)_{22}$ of example (i) is 2.6 times higher than for solid nickel, but at the cost of a low vertical Young's modulus (2.5% of solid nickel).

5. CONCLUSIONS

We have proposed a method to design material microstructures with extreme thermoelastic properties. The optimization procedure has been shown to be very accurate in producing the optimal microstructures. Indeed, the results of this study motivated Gibiansky and Torquato to improve upon the 29-year old Schapery–Rosen–Hashin bounds on the thermal expansion of three-phase media. Our obtained values are close to the Gibiansky–Torquato bounds. We have shown that extreme thermal expansion behavior can be obtained but at the cost of a low bulk modulus. Therefore, there is a tradeoff between extremizing thermal strain coefficients on the one hand and ending up with a stiff material on the other. We have also shown that extreme directional thermal expansion can be obtained by allowing anisotropy of the composites.

For the topology optimization method in general, the results in this paper show, that the method produces designs which are optimal indeed.

In practice, how can our optimally designed materials be manufactured? They may be fabricated (with cell sizes down to a few millimeters) using stereolithography

techniques (e.g. Jacobs, 1992) or using surface micromachining techniques (with cell sizes down to 50 micros) as seen for materials with negative Poisson's ratios in Larsen *et al.* (1997). Furthermore, it will be interesting to examine whether the lessons learned from this continuum analysis can be exploited to optimally design and synthesize materials at the molecular level [e.g. Baughman and Galvão (1993)].

Finally, we note that the method is applicable to design of smart materials (piezoelectric or shape-memory-alloy inclusions). In a future paper, the procedure described here will be used to find the structures that optimize the piezoelectric properties of the material for use as actuators or sensors. The method can also be modified to handle three-dimensional microstructures. The extension to three dimensions is straightforward, but computer time will increase dramatically. Extensions to three dimensions for two material phases have been done in Sigmund (1995) and Sigmund and Torquato (1997).

ACKNOWLEDGEMENTS

We are grateful to L. Gibiansky, P. Pedersen, M. P. Bendsøe, R. Lakes, I. A. Aksay and G. Scherer for helpful discussions. This work was supported by the ARO/MURI Grant DAAH04-95-1-0102 (OS and ST) and Denmark's Technical Research Council (Programme of Research on Computer-Aided Design) (OS).

REFERENCES

ASM (1993) *ASM Handbook, Volume* 2: *Properties and Selection.* The Materials Information Society, U.S.A.

Autio, M., Laitinen, M. and Pramila, A. (1993) Systematic creation of composites with prescribed thermomechanical properties. *Computational Engineering* **3,** 249–259.

Baughman, R. H. and Galvão, D. S. (1993) Crystalline networks with unusual predicted mechanical and thermal properties. *Nature* **365,** 735–737.

Bendsøe, M. P. (1995) *Optimization of Structural Topology, Shape and Material.* Springer.

Bendsøe, M. P. and Kikuchi, N. (1988) Generating optimal topologies in optimal design using a homogenization method. *Computational Methods in Applied Mechanics and Engineering* **71,** 197–224.

Benssousan, A., Lions, J. L. and Papanicolau, G. (1978) *Asymptotic Analysis for Periodic Structures.* North Holland, Amsterdam.

Bourgat, J. F. (1977) Numerical experiments of the homogenization method for operators with periodic coefficients. In *Lecture Notes in Mathematics*, pp. 330–356. Springer Verlag, Berlin.

Christensen, R. M. (1979) *Mechanics of Composite Materials.* John Wiley and Sons.

Collins, E. G. and Richter, S. (1995) Linear-quadratic-gaussian-based controller design for Hubble space telescope. *Journal of Guidance, Control, and Dynamics* **18,** 208–213.

Díaz, A. R., Lipton, R. and Sigmund, O. (1997) Validation of the penalization approach for topology optimization. In preparation.

Díaz, A. R. and Sigmund, O. (1995) Checkerboard patterns in layout optimization. *Structural Optimization* **10,** 40–45.

Francfort, G. and Murat, F. (1986) Homogenization and optimal bounds in linear elasticity. *Archieves of Rational Mechanical Analysis* **94,** 307–334.

Gibiansky, L. V. and Torquato, S. (1997) Thermal expansion of isotropic multi-phase composites and polycrystals. *Journal of the Mechanics and Physics of Solids*, in press.

Grabovsky, Y. and Kohn, R. V. (1995a) Microstructures minimizing the energy of a two phase

elastic composite in two dimensions. I: The confocal ellipse construction. *Journal of the Mechanics and Physics of Solids* **43,** 933–947.

Grabovsky, Y. and Kohn, R. V. (1995b) Microstructures minimizing the energy of a two phase elastic composite in two space dimensions. II: The Vigdergauz microstructure. *Journal of the Mechanics and Physics of Solids* **43,** 949–972.

Guedes, J. M. and Kikuchi, N. (1991) Preprocessing and postprocessing for materials based on the homogenization method with adaptive finite element methods. *Computer Methods in Applied Mechanical Engineering* **83,** 143–198.

Haber, R. B., Jog, C. and Bendsøe, M. P. (1996) A new approach to variable-topology shape optimization using a constraint on perimeter. *Structural Optimization* **11,** 1–12.

Haftka, R. T., Gürdal, Z. and Kamat, M. P. (1990) *Elements of Structural Optimization.* Kluwer, Netherlands.

Hanson, R. J. and Hiebert, K. L. (1981) A sparse linear programming subprogram. Technical Report SAND81-0297, Sandia National Laboratories.

Hashin, Z. and Shtrikman, S. (1963) A variational approach to the theory of the elastic behaviour of multiphase materials. *Journal of the Mechanics and Physics of Solids*, March–April, 127–140.

Hausch, G., Bächer, R. and Hartmann, J. (1989) Influence of thermomechanical treatment on the expansion behavior of invar and superinvar. *Physica B* **161,** 22–24.

Hollister, S. R. and Riemer, B. A. (1992) Digital image based finite element analysis for bone microstructure using conjugate gradient and Gaussian filter techniques. In *SPIE, Volume* 2035 *Mathematical Methods in Medical Imaging II*, pp. 95–106.

Jacobs, P. (1992) *Rapid Prototyping and Manufacturing—Fundamentals of Stereolithography.* SME, Dearborn, MI.

Jog, C. S. and Haber, R. B. (1996) Stability of finite element models for distributed-parameter optimization and topology design. *Computer Methods in Applied Mechanics and Engineering* **130,** 203–226.

Kagaya, H.-M. and Soma, T. (1993) Compression effect on specific heat and thermal expansion of Si and Ge. *Solid State Communications* **85,** 617–621.

Kohn, R. V. and Strang, G. (1986) Optimal design and relaxation of variational problems. *Communications Pure in Applied Mathematics and Mechanics* **39,** 1–25, 139–182, 353–377.

Lakes, R. (1987) Foam structures with negative Poisson's ratio. *Science* **235,** 1038.

Lakes, R. (1993) Materials with structural hierarchy, review article. *Nature* **361,** 511–515.

Larsen, U. D., Sigmund, O. and Bouwstra, S. (1997) Design and fabrication of compliant mechanisms and material structures with negative Poisson's ratio. *Journal of Microelectromechanical Systems*, to appear.

Levin, V. M. (1967) Thermal expansion coefficients of heterogeneous materials. *Mekhanika Tverdoga Tela* **2,** 88–94.

Milton, G. W. and Cherkaev, A. V. (1995) Which elasticity tensors are realizable? *Journal of Engineering Materials and Technology, Transactions of the ASME* **117,** 483–493.

Mlejnik, H. P. and Schirrmacher, R. (1993) An engineering approach to optimal material distribution and shape finding. *Computational Methods in Applied Mechanics and Engineering* **106,** 1–26.

Mullender, M. G., Huiskes, R. and Weihnans, H. (1994) A physiological approach to the simulation of bone remodelling as a self-organizational control process. *Journal of Biomechanics* **11,** 1389–1394.

Parton, V. Z. and Kudryavtsev, B. A. (1993) *Engineering Mechanics of Composite Structures.* CRC Press.

Pedersen, P. (1970) On the minimum mass layout of trusses. In *AGARD Conference Proceedings No.* 36, *Symposium on Structural Optimization*, pp. 189–192.

Press, W. H., Teukolsky, S. A., Vetterling, W. T. and Flannery, B. P. (1992) *Numerical Recipes in Fortran.* Cambridge University Press.

Rodriques, H. and Fernandes, P. (1995) A material bases model for topology optimization of thermoelastic structures. *International Journal for Numerical Methods in Engineering* **38,** 1951–1965.

Rosen, B. W. and Hashin, Z. (1970) Effective thermal expansion and specific heat of composite materials. *International Journal of Engineering Science* **8,** 157–173.
Rozvany, G. I. N., Zhou, M., Birker, T. and Sigmund, O. (1992) Topology optimization using iterative continuum type optimality criteria (COC) methods for discretized systems. In *Topology Design of Structures*, ed. M. P. Bendsøe and C. A. Soares, pp. 273–286. Springer.
Sanchez-Palencia, E. (1980) Non-homogeneous media and vibration theory. In *Lecture Notes in Physics*. Springer Verlag, Berlin.
Schapery, R. A. (1968) Thermal expansion coefficients of composite materials based on energy principles. *Journal of Composite Materials* **2,** 380–404.
Schittkowski, K. (1994) Numerical comparison of non-linear programming algorithms for structural optimization. *Structural Optimization* **7,** 1–19.
Schultz, P. C. and Smyth, K. T. (1970) *Amorphous Materials*, pp. 453–462. Wiley, New York.
Sigmund, O. (1994a) Design of material structures using topology optimization. PhD thesis, Department of Solid Mechanics, Technical University of Denmark.
Sigmund, O. (1994b) Materials with prescribed constitutive parameters: an inverse homogenization problem. *International Journal of Solids and Structures* **31,** 2313–2329.
Sigmund, O. (1995) Tailoring materials with prescribed elastic properties. *Mechanics of Materials* **20,** 351–368.
Sigmund, O. and Torquato, S. (1997) On the design of 1–3 piezocomposites using topology optimization, submitted.
Vigdergauz, S. B. (1989) Regular structures with extremal elastic properties. *Mechanics of Solids* **24,** 57–63.
Vigdergauz, S. B. (1994) Three-dimensional grained composites of extreme thermal properties. *Journal of the Mechanics and Physics of Solids* **42,** 729–740.
Wetherhold, R. C. and Wang, J. (1995) Tailoring thermal deformation by using layered beams. *Composites Science and Technology* **53,** 1–6.
Yang, Z. J., Yewondwossen, M., Lawther, D. W., Ritcey, S., Geldart, D. J. W. and Dunlap, R. A. (1995) Thermal expansion of $Bi_{2.2}Sr_{1.8}CaCu_2O_x$ superconductor single crystals. *Journal of Superconductivity* **8,** 233–239.

APPENDIX A: HOMOGENIZATION THEORY

This appendix summarizes the important equations for computation of the effective thermoelastic properties of a periodic inhomogeneous material using the homogenization theory as developed in Bensoussan *et al.* (1978) and Sanchez-Palencia (1980).

We want to find the effective homogenized thermoelastic tensors $C^{(*)}_{ijkl}$, $\beta^{(*)}_{ij}$ and $\alpha^{(*)}_{ij}$ of a periodic material microstructure described by the rectangular base cell Y. Using the symmetries of the thermoelastic tensors, $C_{ijkl} = C_{jikl} = C_{ijlk} = C_{klij}$, $\beta_{ij} = \beta_{ji}$ and $\alpha_{ij} = \alpha_{ji}$, the anisotropic elasticity tensor has six independent parameters and the thermal expansion tensors have three independent parameters.

Only considering first order terms in the asymptotic expansion, it can be shown that relations for obtaining the effective elasticity, thermal stress and thermal strain tensors can be written in energy forms as

$$C^{(*)}_{pqrs}\varepsilon^{0(kl)}_{pq}\varepsilon^{0(ij)}_{rs} = \frac{1}{Y}\int_Y C_{pqrs}(\varepsilon^{0(kl)}_{pq} - \varepsilon^{(*)}_{pq}(\chi^{kl}))(\varepsilon^{0(ij)}_{rs} - \varepsilon^{(*)}_{rs}(\chi^{ij}))\,\mathrm{d}Y,$$

$$\beta^{(*)}_{kl}\varepsilon^{0(ij)}_{kl} = \frac{1}{Y}\int_Y C_{pqkl}(\alpha_{pq} - \varepsilon^{C}_{pq}(\Gamma))(\varepsilon^{0(ij)}_{kl} - \varepsilon^{(*)}_{kl}(\chi^{ij}))\,\mathrm{d}Y,$$

$$\alpha^{(*)}_{ij} = (C^{(*)}_{ijkl})^{-1}\beta^{(*)}_{kl}, \tag{A.1}$$

where the displacements fields χ^{kl} and Γ are solutions to the following cell problems: find $\chi^{kl} \in V$ and $\Gamma \in V$, such that

$$\int_Y C_{ijpq} \frac{\partial \chi_p^{kl}}{\partial y_q} \frac{\partial v_i}{\partial y_j} \mathrm{d}Y = \int_Y C_{ijpq} \varepsilon_{pq}^{0(kl)} \frac{\partial v_i}{\partial y_j} \mathrm{d}Y, \quad \forall v \in V,$$

$$V = \{v : v \quad \text{is } Y\text{—periodic}\},$$

$$\int_Y C_{ijkl} \frac{\partial \Gamma_k}{\partial y_l} \frac{\partial v_i}{\partial y_j} \mathrm{d}Y = \int_Y \beta_{ij} \frac{\partial v_i}{\partial y_j} \mathrm{d}Y, \quad \forall v \in V,$$

$$V = \{v : v \quad \text{is } Y\text{—periodic}\}. \tag{A.2}$$

The fluctuation strains $\varepsilon^{*(kl)}_{pq}(\chi^{kl})$ and $\varepsilon^{C}_{pq}(\Gamma)$ are defined through the strain-displacement relations $\varepsilon^{(*)}_{pq}(\chi^{kl}) = \frac{1}{2}(\partial \chi_p^{kl}/\partial y_q + \partial \chi_q^{kl}/\partial y_p)$ and $\varepsilon^{C}_{pq}(\Gamma) = \frac{1}{2}(\partial \Gamma_p/\partial y_q + \partial \Gamma_q/\partial y_p)$ and $\varepsilon^{0(kl)}_{pq}$ are three linearly independent test strain fields. In (A.1) and (A.2), C_{ijkl}, β_{ij} and α_{ij} are the locally (dependent on $\mathbf{y}$) varying stiffness, thermal stress and thermal strain tensors, respectively.

As test strain fields $\varepsilon^{0(kl)}_{pq}$ we choose the three unit tensors (in two dimensions) $\varepsilon^{0(11)}_{pq} = (1,0,0,0)$, $\varepsilon^{0(22)}_{pq} = (0,1,0,0)$ and $\varepsilon^{0(12)}_{pq} = (0,0,1,0)$ and $\varepsilon^{0(21)}_{pq}$ can be ignored for symmetry reasons.

The equilibrium equations (A.2), are solved using the finite-element method. The base cell is discretized by finite elements and solving (A.2) means solving a finite-element problem with periodic boundary conditions for the three different prestrain cases: horizontal unit strain, vertical unit strain, shear unit strain as given by the tensors $\varepsilon^{0(kl)}_{pq}$ and for a thermal strain field resulting from the locally varying thermal stress tensor β_{ij}.

Having discretized the base cell by N finite elements, the integrals for the evaluation of the homogenized properties in (A.1) can be evaluated on the element level and the effective properties can be written as the sums

$$C^{(*)}_{ijkl} = \frac{1}{Y} \sum_{e=1}^{N} \int_{Y^e} C^e_{pqrs}(\varepsilon^{0(kl)}_{pq} - \varepsilon^{(*)}_{pq}(\chi^{kl}))(\varepsilon^{0(ij)}_{rs} - \varepsilon^{(*)}_{rs}(\chi^{ij}))\, \mathrm{d}Y^e,$$

$$\beta^{(*)}_{ij} = \frac{1}{Y} \sum_{e=1}^{N} \int_{Y^e} C^e_{pqkl}(\alpha_{pq} - \varepsilon^{C}_{pq}(\Gamma))(\varepsilon^{0(ij)}_{kl} - \varepsilon^{(*)}_{kl}(\chi^{ij}))\, \mathrm{d}Y^e. \tag{A.3}$$

where Y^e is the area of element e.

For a more thorough description of the numerical homogenization procedure and finite-element discretization, the reader is referred to the numerical works of Bourgat (1977) and Guedes and Kikuchi (1991).

To solve the linear system of equations we use a so-called element-by-element preconditioned-conjugate-gradient solver (EBE-PCG). The PCG solver is described in Press *et al.* (1992) and its application to finite-element problems is discussed in Hollister and Riemer (1993), who use the method for the microstructural analysis of human bone structure discretized by up to one million finite elements. The advantages gained by using the EBE-PCG solver for the present design method are multiple. The EBE-PCG solver is an iterative solver using a starting guess for the displacement vector. By using the displacement vector from the preceding design step, computational time can be saved. Furthermore, we do not need an exact solution to the finite-element problem in the beginning of the design sequence, thus we can stop the solver when an approximate solution has been reached. Only in the final iterations of the optimization procedure we need an exact solution and then, the convergence requirements of the solver can be made stricter. Another advantage of the EBE-PCG solver is, that it does not require an assembly of the global stiffness matrix thereby saving storage space, in fact, it is only necessary to store two element stiffness matrices, implying that the stiffness matrix for a particular element can be calculated using (4). Finally, the EBE-PCG solver eliminates problems with increase of bandwidth due to the periodic boundary conditions. Opposing nodes of the base cells are

simply given the same node numbers causing no increase in computational complexity, due to the element-by-element nature of the EBE-PCG solver.

APPENDIX B: SENSITIVITY ANALYSIS

This appendix derives all the sensitivities which are necessary to solve the sequential linear programming problem (10). The sensitivities can be found directly from the strain fields already computed by the homogenization procedure.

The sensitivities of the effective stiffness tensor in (A.1) with respect to design variables x_1^e and x_2^e of element e can be found as

$$\frac{\partial C_{ijkl}^{(*)}}{\partial x_m^e} = \frac{1}{Y}\int_Y \frac{\partial C_{pqrs}}{\partial x_m^e}(\varepsilon_{pq}^{0(kl)} - \varepsilon_{pq}^{(*)}(\chi^{kl}))(\varepsilon_{rs}^{0(ij)} - \varepsilon_{rs}^{(*)}(\chi^{ij}))\,\mathrm{d}Y$$

$$+ \frac{2}{Y}\int_Y C_{pqrs}\frac{\partial(\varepsilon_{pq}^{0(kl)} - \varepsilon_{pq}^{(*)}(\chi^{kl}))}{\partial x_m^e}(\varepsilon_{rs}^{0(ij)} - \varepsilon_{rs}^{(*)}(\chi^{ij}))\,\mathrm{d}Y$$

$$= -\frac{1}{Y}\int_Y \frac{\partial C_{pqrs}}{\partial x_m^e}(\varepsilon_{pq}^{0(kl)} - \varepsilon_{pq}^{(*)}(\chi^{kl}))(\varepsilon_{rs}^{0(ij)} - \varepsilon_{rs}^{(*)}(\chi^{ij}))\,\mathrm{d}Y, \quad m = 1,2, \quad \text{(A.4)}$$

where it was used that

$$\int_Y C_{ijpq}\frac{\partial(\varepsilon_{pq}^{0(kl)} - \varepsilon_{pq}^{(*)}(\chi^{kl}))}{\partial x_m^e}\frac{\partial v_i}{\partial y_j}\,\mathrm{d}Y = -\int_Y \frac{\partial C_{ijpq}}{\partial x_m^e}(\varepsilon_{pq}^{0(kl)} - \varepsilon_{pq}^{(*)}(\chi^{kl}))\frac{\partial v_i}{\partial y_j}\,\mathrm{d}Y, \quad \text{(A.5)}$$

which comes from the differentiation of the equilibrium equations (A.2).

As $\partial C_{ijpq}/\partial x_m^e = \partial C_{ijpq}^e/\partial x_m^e$, the sensitivity of the constitutive tensor (A.4) can be written in the simpler form

$$\frac{\partial C_{ijkl}^{(*)}}{\partial x_m^e} = -\frac{1}{Y}\int_{Y^e} \frac{\partial C_{pqrs}^e}{\partial x_m^e}(\varepsilon_{pq}^{0(kl)} - \varepsilon_{pq}^{(*)}(\chi^{kl}))(\varepsilon_{rs}^{0(ij)} - \varepsilon_{rs}^{(*)}(\chi^{ij}))\,\mathrm{d}Y, \quad m = 1,2, \quad \text{(A.6)}$$

which is seen to be dependent on local (element) quantities only.

It is hereby proved that the sensitivities can be calculated analytically by using the strain fields already calculated for the homogenization analysis. The sensitivity analysis derived here, corresponds to the well known "adjoint sensitivity analysis" as reviewed in e.g. Haftka *et al.* (1990).

The sensitivities of the local stiffness tensor are

$$\frac{\partial C_{ijkl}^e}{\partial x_1^e} = p(x_1^e)^{\eta-1}[(1-x_2^e)C_{ijkl}^{(1)} + x_2^e C_{ijkl}^{(2)}] \quad \text{and} \quad \frac{\partial C_{ijkl}^e}{\partial x_2^e} = (x_1^e)^{\eta}(-C_{ijkl}^{(1)} + C_{ijkl}^{(2)}). \quad \text{(A.7)}$$

Similar to the derivation of sensitivity of the stiffness tensor (A.4), the sensitivity of the effective thermal stress tensor with respect to design variable x_1^e in (A.3) can be found as

$$\frac{\partial \beta_{ij}^{(*)}}{\partial x_1^e} = -\frac{1}{Y}\int_{Y^e} \frac{\partial C_{pqkl}^e}{\partial x_1^e}(\alpha_{pq} - \varepsilon_{pq}^C(\Gamma))(\varepsilon_{kl}^{0(ij)} - \varepsilon_{kl}^{(*)}(\chi^{ij}))\,\mathrm{d}Y^e, \quad \text{(A.8)}$$

where it was used that the thermal test field α_{ij} is independent of design variable x_1^e (i.e. $\partial \alpha_{ij}/\partial x_1^e = 0$).

As α_{ij} is dependent on design variable x_2^e (i.e. $\partial \alpha_{ij}^e/\partial x_2^e = -\alpha_{ij}^{(1)} + \alpha_{ij}^{(2)}$), sensitivity of the effective thermal tensor with respect to design variable x_2^e in (A.3) has an extra term

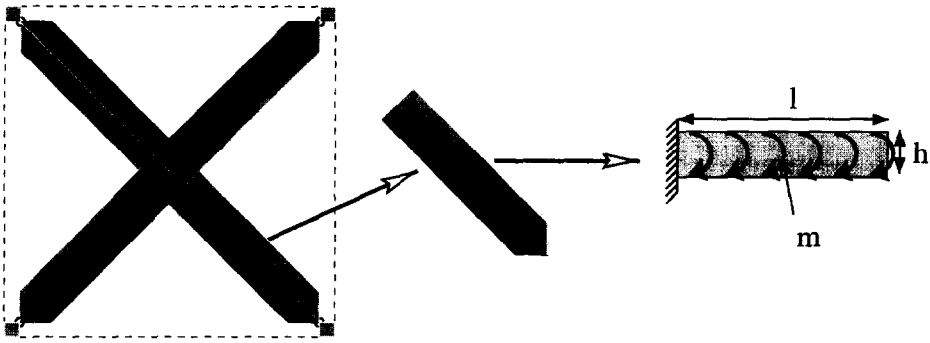

Fig. A1. Idealization of the cross microstructure from Fig. 8.

$$\frac{\partial \beta_{ij}^{(*)}}{\partial x_2^e} = -\frac{1}{Y}\int_{Y^e} \frac{\partial C_{pqkl}^e}{\partial x_2^e}(\alpha_{pq} - \varepsilon_{pq}^C(\Gamma))(\varepsilon_{kl}^{0(ij)} - \varepsilon_{kl}^{(*)}(\chi^{ij}))\,\mathrm{d}Y^e$$

$$+\frac{1}{Y}\int_{Y^e} C_{pqkl}^e \frac{\partial \alpha_{pq}^e}{\partial x_2^e}(\varepsilon_{kl}^{0(ij)} - \varepsilon_{kl}^{(*)}(\chi^{ij}))\,\mathrm{d}Y^e. \quad \text{(A.9)}$$

Sensitivities of the effective thermal strain tensor $\alpha_{ij}^{(*)}$ with respect to design variables x_1^e and x_2^e are found by differentiating (A.1) as follows

$$\frac{\partial \alpha_{ij}^{(*)}}{\partial x_m^e} = \frac{\partial (C_{ijkl}^{(*)})^{-1}}{\partial x_m^e}\beta_{kl}^{(*)} + (C_{ijkl}^{(*)})^{-1}\frac{\partial \beta_{kl}^{(*)}}{\partial x_m^e}, \quad m = 1,2. \quad \text{(A.10)}$$

Finally, the sensitivities of the volume fractions (5) with respect to design variables x_1^e and x_2^e are

$$\partial c^{(1)}/\partial x_1^e = (1-x_2^e)\,Y^e/Y, \quad \partial c^{(1)}/\partial x_2^e = x_1^e\,Y^e/Y, \quad \partial c^{(2)}/\partial x_1^e = x_2^e\,Y^e/Y, \quad \partial c^{(2)}/\partial x_2^e = x_1^e\,Y^e/Y. \quad \text{(A.11)}$$

APPENDIX C: BEAM MODEL OF THERMAL ACTUATOR EXAMPLE

To check the results obtained with the topology optimization algorithm, this appendix calculates the effective thermal strain tensor for the "maximization of vertical expansion" (Fig. 8) example (e) using a simple beam model.

The cross-like topology from Fig. 8 can be idealized as seen in Fig. A.1. In the inter-presentation we assume that each of the four legs are slender beams of height h, width $w = 1$ and length $l = \sqrt{2}/2$. The four beam legs are joined together at the center of the cell and connected to neighboring cells with ideal moment-free hinges.

The thermal strain coefficient of the beam model can be found by calculating the bending and elongation of each "leg" and projecting these displacements to the horizontal and vertical directions. Using Bernoulli–Euler beam theory, the strain across the thickness of a beam varies with the distance from the neutral axis as $\varepsilon_x = y/r$, where ε_x is the strain in the x-direction (horizontal) and r is the radius of curvature. Using Hooke's law, the stress in the x-direction of the beam is $\sigma_x = E\varepsilon_x = Ey/r$. The thermal expansion of the two layers can be seen as an applied thermal stress to the two layers, i.e. $\sigma_{T(i)} = E\alpha_i$ $(i = 1,2)$. To find the beam moment–curvature relationship, resulting moments about the transverse beam-axis are summed to give

$$w\int_{-h/2}^{h/2}\sigma_T y\,dy = w\int_{-h/2}^{h/2}\sigma_x y\,dy \tag{A.12}$$

or

$$w\int_{-h/2}^{0}E\alpha^{(1)}y\,dy - w\int_{0}^{h/2}E\alpha^{(2)}y\,dy = w\int_{-h/2}^{h/2}E\frac{y^2}{r}dy. \tag{A.13}$$

Equation (A.13) can be evaluated as

$$w\frac{1}{8}Eh^2\alpha^{(1)}y - w\frac{1}{8}Eh^2\alpha^{(2)}y = wE\frac{h^3}{12r}. \tag{A.14}$$

Using the approximation $d^2y/dx^2 \approx 1/r$, the differential equation for bending of the beam can be found as

$$\frac{d^2y}{dx^2} = \frac{1}{r} = \frac{3(\alpha^{(1)}-\alpha^{(2)})}{2h}. \tag{A.15}$$

Integrating (A.15) twice with respect to x, we get the vertical displacement at the tip of the cantilever

$$u_y = \frac{3l^2(\alpha^{(1)}-\alpha^{(2)})}{4h}. \tag{A.16}$$

The displacement in the x-direction is simply the average elongation

$$u_x = l(\alpha^{(1)}+\alpha^{(2)})/2. \tag{A.17}$$

Rotating the leg 45° the resulting deflection of one leg in the horizontal and vertical directions are

$$u_h = \frac{\sqrt{2}}{2}(u_x+u_y) \quad \text{and} \quad u_v = \frac{\sqrt{2}}{2}(-u_x+u_y). \tag{A.18}$$

The effective thermal strain coefficients are the relative displacements of the whole cross in the horizontal and vertical directions, respectively

$$\alpha_{11}^{(*)} = \frac{2u_h}{l_x} = \frac{\sqrt{2}(u_x+u_y)}{l_x} = \frac{\sqrt{2}}{l_x}\left(l(\alpha^{(1)}+\alpha^{(2)})/2 + \frac{3l^2(\alpha^{(1)}-\alpha^{(2)})}{4h}\right),$$

$$\alpha_{22}^{(*)} = -\frac{2u_v}{l_y} = -\frac{\sqrt{2}(-u_x+u_y)}{l_y} = \frac{\sqrt{2}}{l_y}\left(l(\alpha^{(1)}+\alpha^{(2)})/2 - \frac{3l^2(\alpha^{(1)}-\alpha^{(2)})}{4h}\right). \tag{A.19}$$

Finally, by inserting $l = \sqrt{2}/2$, we get

$$\alpha_{11}^{(*)} = \frac{1}{2l_x}(\alpha^{(1)}+\alpha^{(2)}) \pm \frac{3\sqrt{2}}{8hl_x}(\alpha^{(1)}-\alpha^{(2)}). \tag{A.20}$$

The thickness of the legs in Fig. 8 is estimated to $h = 0.18$. Inserting this value together with material data in (A.20), we get $\alpha_{11}^{(*)}/\alpha^{(1)} = -21$ and $\alpha_{22}^{(*)}/\alpha^{(2)} = 32$.

Again using simple beam analysis, the effective bulk modulus can be found as $k^{(*)} \approx 16Ewh^3$. Inserting $h = 0.18$ and $w = 1$, we get $k^{(*)}/k^{(1)} \approx 0.085$.